Conversion of plastic solid wastes into carbon nanotubes: effect of operating conditions

ISABELLA VERONICA KOSLINSKI FREITAS

Final dissertation report submitted to ***Escola Superior de Tecnologia e Gestão*** *of* ***Instituto Politécnico de Bragança*** *to obtain the Master's Degree in* ***Chemical Engineering*** *in the scope of the double diploma with the* ***Universidade Tecnológica Federal do Paraná – Campus Ponta Grossa***

Work oriented by:

Prof. Dr. Helder Teixeira Gomes

Profª. Drª. Giane Gonçalves Lenzi

Dr. Jose Luis Díaz de Tuesta Triviño

Bragança

2021

ACKNOWLEDGEMENTS

Many people have facilitated the preparation of this work for both practical and scientific support, as well as in an emotional and affective way. In this sense, I extend my acknowledgments to all who have been with me throughout this research, in special to my parents and my friends.

Thanks to my supervisors, professor Dr. Helder Teixeira Gomes of Instituto Politécnico de Bragança (IPB), professor Drª. Giane Gonçalves Lenzi of Universidade Tecnológica Federal do Paraná (UTFPR-PG) and Dr. Jose Luis Díaz de Tuesta of Instituto Politécnico de Bragança (IPB), for helping me with my work and for clearing all doubts I had. The group meetings and the guidance that was given was very enriching, and the knowledge that was transferred will never be forgotten.

I thank the researchers that were always with me during the lab days, Adriano dos Santos Silva, Ana Paula Ferreira da Silva and Fernanda Fontana Roman, for the availability and energy to support and teach me everything I needed. Also, the technician of the Chemical Processes Laboratory, Eng. Maria João Almeida Pinto Santos Afonso, for the help and suggestions given.

Finally, I thank UTFPR and IPB for all the structure, receptibility and opportunities that made me grow and develop a lot as a person with this work.

This work is a result of project PLASTIC_TO_FUEL&MAT, with reference POCI 01 0145-FEDER-031439 and CIMO - UIDB/00690/2020 financed through FCT/MCTES (PIDDAC).

Abstract

An efficient treatment of plastic waste brings remarkable environmental, social and economic benefits. Therefore, this work proposes the recovery of plastic waste by its conversion to carbon nanotubes (CNTs) by sequential pyrolysis and chemical vapor deposition (CVD). For this purpose, an alumina-supported iron material, prepared by the sol-gel method, was used as catalyst in chemical vapor deposition. This method allows to control the size of the formed carbon nanostructures. To understand the variables affecting the proportion and to maximize material yield, catalyst, flow rate and temperature at which CVD will occur were studied in this work. Three types of pure polymers were used as carbon precursors: low-density polyethylene (LDPE), high-density polyethylene (HDPE) and polypropylene (PP), as well as a mixture of them. The best conditions for the formation of CNTs was found to be 40 mL/min of nitrogen inflow and 800 °C for the polymers, with the following yields, respectively: 16.9 (LDPE), 8.5 (HDPE), 6.7 (PP) and 8.9 (MIX) %. The obtained samples were purified with 50 % H_2SO_4. Ash content, acidity and basicity, S_{BET}, XRD and FT-IR, were considered for the characterization of the materials. In the ashes, the purification removed a good part of the inorganic content, as the acid-base titration it demonstrated that the CNTs had an acidic character confirmed by the FT-IR. XRD revealed that the iron phase in the catalyst produced was Fe_2O_3, and the determination of the ash content confirmed the XRD results by the red color of the material at the end. And by porosimetry analysis, they were shown to be materials within the range of 159-242 m^2/g, with their adsorption and desorption graphs resulting in a mesoporous material, characteristic of nanotubes.

Keywords: Carbon nanotubes; chemical vapour deposition; plastic waste; solid waste management; recovery technologies.

Resumo

Um tratamento eficiente de resíduos plásticos traz benefícios ambientais, sociais e econômicos notáveis. Portanto, neste trabalho é proposta a valorização de resíduos plásticos em sua conversão para nanotubos de carbono (CNTs). Para que o processo ocorra, é necessário um catalisador que contenha metal de transição. Então é feito um catalisador de ferro suportado em alumina, Fe_2O_4/Al_2O_3, pelo método de sol gel no qual seu rendimento foi em torno de 25% de ferro. O método para formação dos nanotubos é a deposição química em fase vapor (CVD) que permite realizar o controle do tamanho das nanoestruturas de carbono formadas, com o uso de catalisadores adequados ao processo. Tanto para o controle do tamanho quanto para maior rendimento do material são diversas variáveis, as estudadas serão: o catalisador, o caudal e a temperatura que ocorrerá o CVD. Também serão usados três tipos de polímeros: polietileno de baixa densidade (LDPE), polietileno de alta densidade (HDPE) e polipropileno (PP), e uma mistura (MIX) entre eles. No qual a melhor condição para formação dos CNTs foi 40 mL/min de nitrogênio e a 800 °C com os seguintes rendimentos: 16.9 (LDPE), 8.5 (HDPE), 6.7 (PP) and 8.9 (MIX) %, respectivamente. A maioria das amostras foram purificadas com 50 % de ácido sulfúrico. Cinzas, acidez e basicidade, S_{BET}, DRX, e FT-IR foram os métodos de caracterização. Nas cinzas, a purificação retirou boa parte do conteúdo inorgânico, assim como pela titulação ácido-base, demostrou que os CNTs tiveram caráter ácido comprovado pelo FT-IR. O DRX mostrou ser Fe_2O_3 o catalisador produzido, e com as cinzas provou ser o mesmo material pela coloração avermelhada. E por análise de porosimetria demonstrou serem materiais dentro do intervalo de 159-242 m^2/g, com seus gráficos de adsorção e dessorção resultando um material mesoporoso, característico de nanotubos.

Palavras chave: Nanotubos de carbono; deposição química de vapor; resíduos plásticos; gestão de resíduos sólidos; tecnologias de valorização.

CONTENTS

List of tables

List of figures

Acronyms

CCVD	Catalytic Chemical Vapor Deposition.
CNT	Carbon nanotubes.
CVD	Chemical Vapor Deposition.
FT-IR	Fourier transformed infrared spectroscopy
HDPE	High Density Polyethylene.
IUPAC	International Union of Pure and Applied Chemistry
LDPE	Low Density Polyethylene.
MA-PP	Malleated Polypropylene.
MSW	Municipal Solid Waste.
MWCNTs	Multi-walled carbonnanotubes.
PE	Polyethylene.
PET	Polyethylene terephthalate.
PP	Polypropylene.
PS	Polystyrene.
PSW	Plastic Solid Waste.
PVC	Polyvinyl chloride.
PVD	Physical Vapor Deposition.
SWCNTs	Single-walled carbonnanotubes.
XRD	X-ray diffraction

1 Introduction

Before the Second World War, plastic production was almost insignificant from a historical perspective. It was with the continuation of the Second World War that plastic production started to increase due to growing shortages of other materials. After the end of the war, plastic producers started to look for new markets for their newly created production capacity. The unprecedented economic growth of the postwar decades, together with the emergence of the modern consumer society, has led to the rapid and sustained growth of global plastic production, for applications such as packaging, building and construction, transportation, renewable energy, medical devices or even sports. The plastics family is composed of a myriad of purpose and resource-efficient materials that allow society to have access to clean water and effective sewage systems, transport, global connectivity, safe food, energy-efficient homes, renewable energies or affordable and hygienic healthcare.

The increase in population and economic growth adds to the demand for plastic and for the feedstock chemicals used in their production. In 2018, 25% of plastic post-consumer waste was still sent to landfill, being China the largest global plastic producer, followed by Europe and North America[1].

According to the World Economic Forum, today, about 4-8% of annual global oil consumption is associated with plastics. If this reliance on plastics persists, plastics will account for 20% of oil consumption by 2050. Plastics refining is greenhouse-gas intensive. For example, the CO_2 emissions from ethylene production are projected to expand by 34% between 2015 and 2030. These emissions are accounted since the extraction and transportation of raw materials of plastic until plastic waste management. In the first half of April 2020, with the coronavirus pandemic, these emissions dropped to 12% in the US, 11% in the EU, 9% in India and 1.7% in China, but is not the solution for the real problem, this reduction could continue for more time to see any change.

The number of biodegradable plastics has increased in the past few decades due to their reputation as an environmentally friendly product. However, these products are not considered as a resolution to the accumulation problem, since biodegradation does not degrade the whole plastic products, also ending up in the solid waste main stream[2]. The diversity in plastic composition, obliging separation, sorting and cleaning costs, are the

biggest challenge for reuse and recycling. The high level of impurities and additives in the waste plastics will downgrade the quality and usability of the recycled products[3].

The concept of circular economy is an economically attractive measure for waste management that can be applied to different stages of the value chain: design, production, use (and reuse) and end-of-life, and may include several recycling techniques (either biologically, mechanically, chemically or thermally). Enabling a substitution of raw materials with post-consumer materials, recycling is one of the favorite methods in waste management, but the percentage is still low, as long as landfilling is considered as a common solution[4]. The production of high value products from recycled waste plastics would significantly promote a rise in collection and recycling rates[5].

The most common proposed solutions for the management of Municipal Solid Waste (MSW) are incineration and mechanical recycling. However, incineration contributes to pollution, caused by toxic and harmful emissions. Besides, both processes are expensive and may not be economically viable in different situations. A feasible alternative is the preparation of carbon nanomaterials, using plastic waste as carbon precursors, as it allows combining the reduction of wastes disposed in landfills with the potential benefits of carbon materials[6].

In this study, a systematic review was performed to assess the literature currently available on the production of carbon nanotubes obtained from plastic solid wastes though pyrolysis and Chemical Vapor Deposition (CVD) methods.

2 Plastics

Plastics are composed of synthetic organic polymers, which contain 60–90% of carbon, produced from fossil fuel, coal, oil and natural gas. Polymers are large molecules consisting of many equal or similar subunits bonded together. Plastic materials have malleability or plasticity during manufacture, allowing it to be cast, pressed or extruded into a variety of shapes - such as films, fibers, plates, tubes, bottles, boxes and much more[7].

In the long term, plastic production must decouple from fossil feedstock, allowing in the future that the production of most plastics will consider alternative feedstocks, such as recycled oils or secondary plastics, responsibly sourced biomassws or even CO_2 [7].

Due to the diversity of properties found in plastics, they are normally separated based on the material's response to heating into thermoplastics and thermosets. Thermoplastic is a family group of plastics that stands out for having the ability to be melted when heated and hardened when cooled cyclically. Thus, these materials can be heated, modeled and cooled repeatedly, defining reversibility in the process[8], as polyethylene (PE), polypropylene (PP), polyvinyl chloride (PVC), polyethylene terephthalate (PET), polystyrene (PS) and others. Thermoset plastics undergo a chemical change when heated, which favors the formation of a three-dimensional network and therefore cannot be remodeled, as polyurethane (PUR), epoxy resins, silicone, phenolic resins, acrylic resins, unsaturated polyester and melamine[9].

2.1 Plastics Management in Europe

Since 2006, the amount of plastic waste sent to recycling has doubled. However, in 2018, 25% of the plastic post-consumer waste was still sent to landfills, although in the same time the energy recovery had an increase of 77% [7].

Figure 1 shows the most demanded plastics in Europe (EU28+NO/CH), namely: PS+EPS 6.6%, followed by PET 7.9%, PUR 7.9%, PVC 10%, HDPE 12.4%, LDPE 17.4%, PP 19.4% and, finally, other types of plastics with 11.3%.

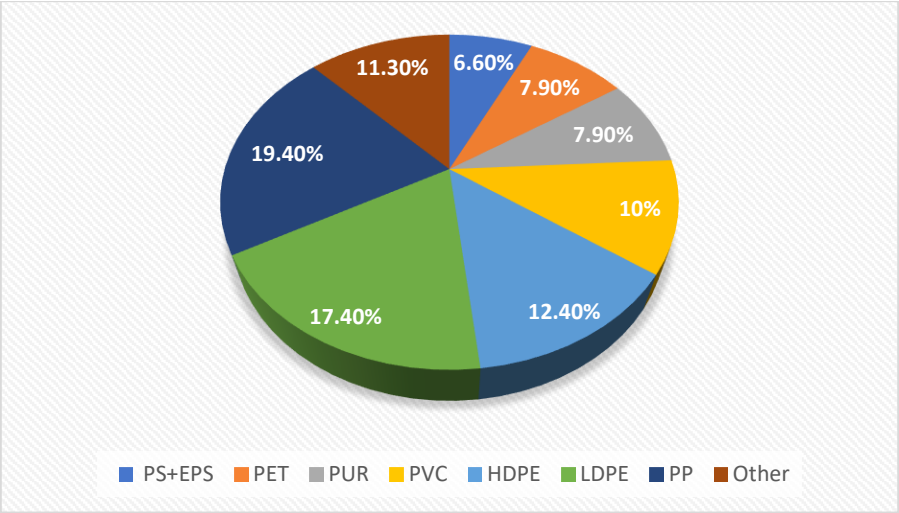

Figure 1. The most used plastic in EU. Source: PlasticsEurope,2020.[7]

The European Strategy for Plastics in a Circular Economy, adopted on January 2018, aims to transform the way plastic products are designed, used, produced and recycled in the EU. Better design of plastic products, higher plastic waste recycling rates, more and better quality, will help boosting the market for recycled plastics. It will deliver greater added value for a more competitive and resilient plastics industry.

In 2019, Europe reached 16% of the world's plastics production and the industry reached a positive trade balance of more than 13 billion euros. Plastic waste exports outside the EU have decreased by 39% from 2016 to 2018[7]. The world and Europe production of plastics are represented in Figure 2.

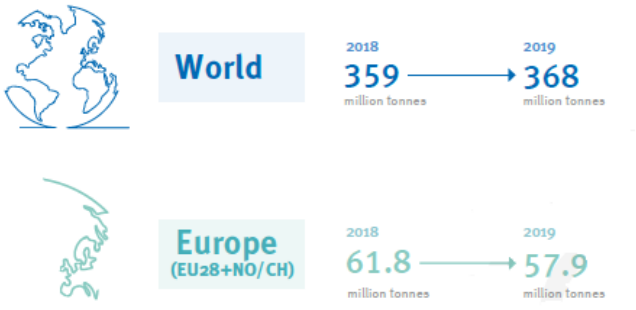

Figure 2. World and EU Plastics Production Data. Souce: PlascticsEurope, 2020[7].

The EU is restricting plastic pollution and member states have agreed to achieve a 90% collection target for plastic bottles by 2029, the plastic bottles needing to contain at least 25% of recycled content by 2025 and 30% by 2030[10].

The new Directive (EU) 2019/852 on Packaging and Packaging Waste sets higher recycling targets per material (50% for plastic packaging by 2025 and 55% by 2030), coupled with a new calculation method of recycling performances, contributing to moving Europe out of the crisis and laying the foundations for more sustainable and inclusive growth[7]. In October 2019, the European Council presented the 8th Environment Action Programme (EAP) which offers political guidance for the EU's environment and climate change policies for the period 2021 – 2030. The 8th EAP determines in its choices that climate change, pollution, loss of biodiversity and the growing demand for natural resources are jeopardizing the well-being and prospects of current and future generations. The European Commission is also invited to present a new action plan for the circular economy, which means basically, sharing, leasing, reusing, repairing, refurbishing and recycling existing materials and products if possible. The European Commission has adopted a new Circular Economy Action Plan with present measures aimed to:

- Make sustainable products the norm in the EU.
- Empower consumers and public buyers.
- Focus on the sectors that use most resources and where the potential for circularity is high such as electronics, batteries and vehicles, packaging, plastics, textiles, construction and buildings, food, water and nutrients.
- Ensure less waste.
- Make circularity work for people, regions and cities.
- Lead global efforts on circular economy.

In Portugal, some strategies were implanted across the country as the ban of plastic bags, cutlery and trays for bread, fruits and vegetables. Also incineration rate on household waste, which can be applied only to recyclable waste or depending on the type of waste, sorting residual or non-separated waste to recover more plastic packaging waste, as well as sending unpacked plastic waste for recycling[11].

The effort from the EU is an indicator that the actual preoccupation is alarming, showing concern about the future and being possible to observe that besides important for the plastics economy, those efforts are also necessary for the welfare and technological advances.

2.2 Strategies of treatment

In municipal solid waste (MSW) management, especially in the management of plastic solid waste (PSW), four treatment methods are normally considered[2,12], as represented in Figure 3.

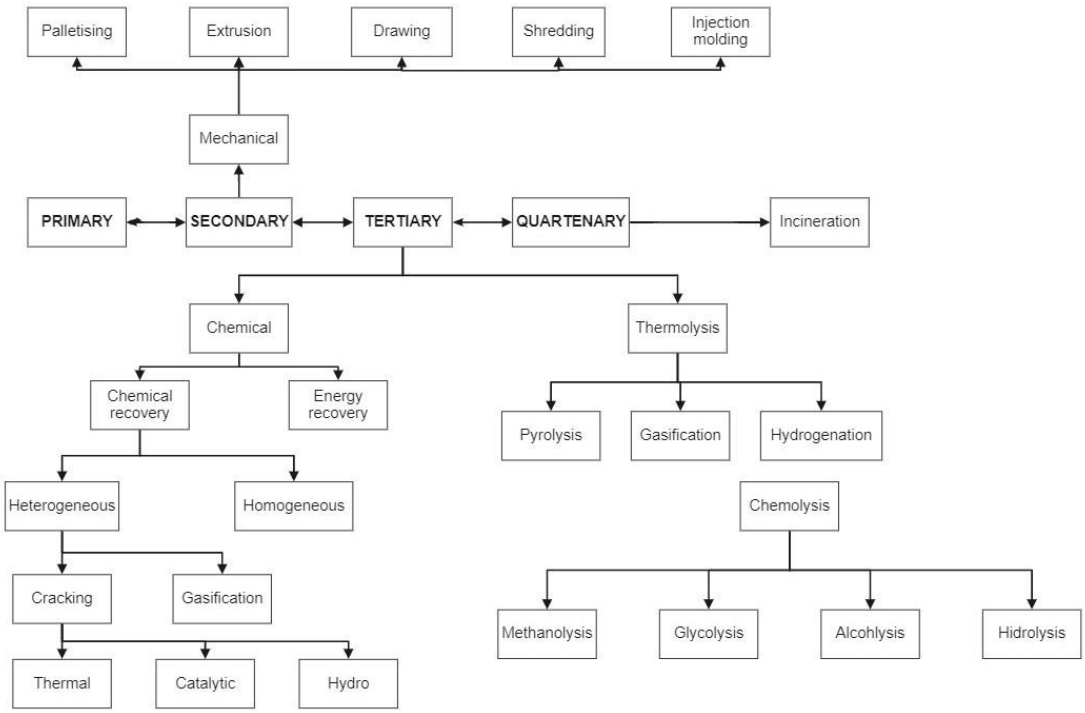

Figure 3. Approaches for recycling. Adapted from Singh et al, 2016[2].

Primary recycling or closed-loop process is applied for clean or semi-clean waste. Thermoplastics can be used in this option. Generally, this method is used in the same industry that makes the scrap. Secondary recycling or mechanical recycling involves physical processes in the structure and it is interesting since allows the plastic to be used as a raw material in other plastic products[12]. Both primary and secondary methods are difficult to deal due to the heterogeneity of PSW.

Tertiary recycling consists in the application of chemical processes that will change the plastic structure. Some chemical methods can be applied in this recycling, such as solvolysis, thermolysis, hydrolysis, glycolysis, aminolysis, gasification, hydrogenation, viscosity breaking, pyrolysis/thermal cracking, steam or catalytic cracking, and the use of PSW as a reducing agent in blast furnaces[13].

Quaternary recycling is based on the high calorific value of PSWs, this process working for energy recovery of steam, heat and electricity from waste through incineration. There are other methods as co-incineration by the direct combustion process of a single stage of waste, fluidized bed and two-stage incineration, rotary combustion, and cement kiln[13]. This option is not attractive due to the emissions to the atmosphere.

Thermal treatments of PSW for chemical products have been considered as promising methods to deal with waste plastic/hydrocarbons-related environmental problems and exploit the full potential of waste plastics recycling. Pyrolysis and gasification have been used to convert PSW into gases, liquid and carbon nanotubes[5], *i.e.*, growing materials from pyrolyzing hydrocarbons to the gas phase and depositing them onto solid surfaces[14]. Besides reducing and upcycling waste plastics, this process provides a green alternative[15].

The comparison with other MSW treatment methods shows pyrolysis as the best between them. Following the European rules for a more circular economy and resulting in monomers that can be used in different ways, being more tolerant than mechanical recycling when it comes to contaminated or mixed plastic waste[16].

2.2.1 Pyrolysis of plastic solid waste

Pyrolysis is a process conducted under inert atmosphere to break down molecular polymer into small products. This method reduces the carbon footprint of processes since uses atmosphere without oxygen, not forming CO and CO_2. The basic products are solid (charcoal), liquid (fuel) and noncondensable gases (methane, hydrogen, propane, propene, ethane, ethene and butane). The liquid oil may be used as an alternative source of energy[17], the char can be upgraded to form CNT[16] and the gases obtained can be used for the synthesis of CNT's over metal-based catalysts in a second stage[18]. Most researchers focus on optimizing the liquid oil quality and maximizing yield by producing new materials.

Pyrolysis and gasification are the most effective thermo-chemical methods for upcycling waste plastics[16]. Thermal pyrolysis requires temperatures higher than 400 °C, producing long carbon chains. Catalytic pyrolysis allow to decrease the residence time, affecting the product selectivity and making the cracking reaction faster[2,19].

Several factors influence the pyrolysis including the feedstock composition, operational factors (temperature[20], retention time[21], feedstock composition[22], catalyst[6],

moisture content[23], heating rate[24] and particle size[25]) and type of furnace. Some of current research works with catalytic pyrolysis are represented in Table 1.

Table 1. Catalysts used in catalytic pyrolysis

Catalysts	**Authors**
$Ni/Ce/Al_2O_3$	Balasundram et al, 2021[26]
ZSM-5 Zeolite	Eimontas et al, 2021[30]
Ni/ZSM-5	Gałko et al, 2021[27]
HZSM-11	Kim et al, 2021[28]
Hicken egg shell	Liew et al, 2021[32]
Nano zeolite particle	Moorthi et al, 2021[34]
ZSM-5 Zeolite	Novarini et al, 2021[33]
Sulfonated carbon	Premalatha et al, 2021[31]
Zeolite ZAA	Rusnadi et al, 2021[29]

2.3 Carbon nanotubes

Nanotechnology is a wide area of research and advanced manufacturing technology has been rising worldwide. It deals with a variety of materials produced at the nanometer scale through different chemical and physical methods. The field with the most increasing interest in nanotechnology is nanostructured materials or nanomaterials, which have dimensions below 100 nm[26].

Carbon nanostructures comprise allotropes of the carbon element, which is defined by different spatial arrangements of carbon atoms at the nanoscale, including diamond, graphite, fullerene, nanofibers, graphene, CNTs and others[26]. Among them, carbon nanotubes are known to contain one or several concentric graphite-like layers, consisting of coaxial tubular graphene sheets that are closed at each end by half of a fullerene molecule[14,27]. The atoms are chemically bonded with sp2 bonds, which are stronger than the sp3 bonds in diamonds.

Two types of CNTs are classified according to the number of carbon layers, see in Figure 4, the most know are single-walled carbon nanotubes (SWCNTs) and multi-walled

carbon nanotubes (MWCNTs). SWCNTs consist of a single graphene layer with a diameter varying between 0.4 and 2 nm and usually occurs as hexagonal-packed bundles[26]. Its properties are dependent on the diameter and chirality defined by the chiral vector (how the nanotube is rolled)[28] being superconductor. MWCNTs are comprised of two or several cylinders, each made up of graphene sheets. The diameter varies from 1 to 3 nm. MWNTs are produced in large quantities whereas developing industry-scale SWNTs still requires improvement[28].

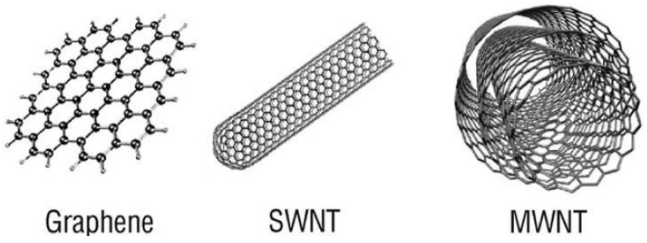

Figure 4. Carbon based materials. Source : Zhuo et al, 2014[14]. Free Access.

There are other types of CNTs, as polymerized SWNT, nanotorus and nanobuds, as can be observed in Figure 5. Polymerized SWNTs is the solid-state manifestation of fullerenes and related compounds and materials. Many single-walled nanotubes intertwine to form polymerized SWNTs, which are comparable to diamond in terms of hardness. Nanotorus have magnetic moments 1000 times larger than previously expected for a certain specific radius and theoretically described as a donut shape. Carbon Nanobuds are a newly discovered material, combining carbon nanotubes and fullerenes[29].

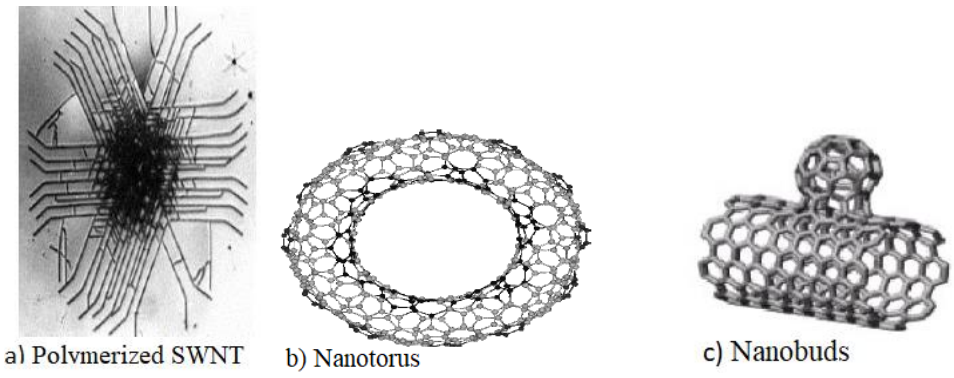

Figure 5. a) Polymerized SWNT, b) Nanotorus and c) Nanobuds. Source: Rajesh Purohit et al, 2014[29]. Image reproduced with permission of the rights holder, Elsevier.

The mechanical tensile strength of CNTs can be 400 times that of steel, they are also very light weight, and the thermal conductivity is better than that of diamond. In addition, CNTs are extremely resistant to corrosion due to their high chemical stability. They are

essential for applications in the field of nanoelectronics where many of these applications depend on chirality and their diameter. The presence of electronically and chemically active defects and impurities can alter these properties. Due to their extraordinary mechanical, electrical, and optical properties, there are many kinds of research and products made of CNTs. Some of those applications are[27]:

- Industrial sectors as a filler material in composites to improve mechanical properties or electrical conductivity.
- Electromagnetic and microwave absorbing coatings.
- Thermal interface materials.
- Ionic and electronic transport devices such as actuators, supercapacitors, batteries, fibers and sensors.
- Energy storage and energy conversion devices.
- Radiation sources.
- Nanometer-sized semiconductor devices.
- Emission displays, X-ray tubes, electron sources for microscopy and lithography, gas discharge tubes, vacuum microwave amplifiers and scanning probe tips.
- To tune their electronic response, as a transistor or logic element.
- Interconnect applications.
- Used as membranes for water purification and gas separation.
- Include biomolecule, drug and drug delivery to the targeted organs, biosensor diagnostic and analysis[26].

There are various methods of synthesis of CNTs, such as arc discharge, CVD, laser ablation, flame synthesis, high pressure carbon monoxide, electrolysis and hidrothermal[14,26], among others, as represented in Figure 6.

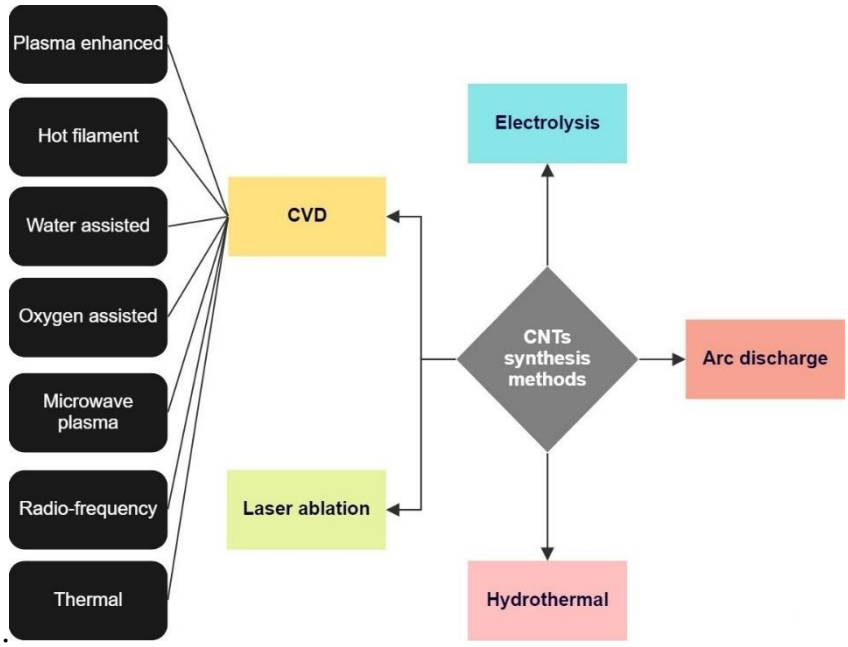

Figure 6. Methods for CNTs synthesis.

These technics of production involve complex experimental setups, adding the cost of production, as they require expensive processing conditions, including gases as feedstock, high vacuum levels, high temperature, inert atmosphere and long processing times. However, in the past two decades, the method widely accepted in the synthesis of CNTs has been the CVD method due to its continuous mass production, simplicity and low cost[5].

2.4 Chemical Vapor Deposition

The CVD process is a deposition method to represent heterogeneous reactions in which both solid and volatile reaction products are formed from a volatile precursor[30] to form a stable film on a substrate in a surface, produced by the reaction of chemicals from the gaseous state[18]. The synthesis process is based on the action of a catalyst to decompose a carbon source, in this study the plastic waste, at a sufficiently high temperature in a tubular reactor[31]. This method is the much-reported process for the production of CNTs using the non-condensable gases from the pyrolysis process[27] and is the most versatile and promising technique in terms of bulk production and direct device integration[32].

This method was developed in the 1960s for J.M. Blocher at the symposium of the Electrochemical Society in Houston, for detached the deposition of thin film based on chemical reactions to the physical process (PVD) and has been successfully used in the production of carbon fibers and carbon nanofibers. Just in a few years, CVD emerged as

a potential method for the synthesis and large-scale production of CNT's in different forms[26]. Furthermore, the process is cheap, versatile and, consequently, requires a carbon source in any state, the substrate as a support material and catalyst in nanometer size.

In the CVD process, the catalyst, composed of transition metals supported on either porous or flat supports, is first heated to high temperatures (700 to 1000 °C). Another common option is using metal nanoparticles formed in the gas phase and floating in the flow of the feeding gas. The introduction of precursor gas containing the carbon source into the furnace is fundamental. There are several choices of furnace configurations, a horizontal furnace setup is shown in Figure 7, vertical furnaces and fluidized bed reactors (a variation of the vertical furnace) can also be considered[31].

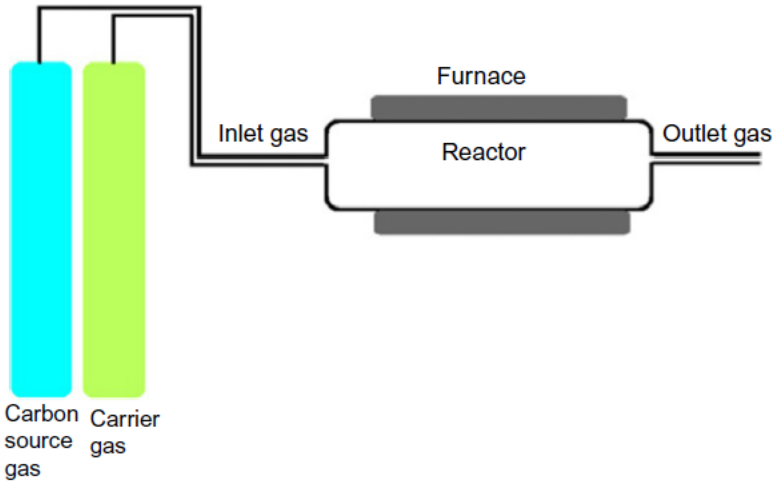

Figure 7. Schematic of the typical CVD process furnace. Source: F. Ghaemi et al, 2018[31]. Image reproduced with permission of the rights holder, Elsevier.

Along with a carbon source, there is the need for a carrier gas in the process, such as argon or nitrogen, among others[28]. The process begins at high temperatures, when the catalyst (metal) decomposes the carbon source (usually a hydrocarbon gas) to form carbon and hydrogen due to the presence of heat or plasma[31]. Hydrogen is charged along with the passing carrier gas or reducing gas, and carbon gets dissolved into the metal followed by their adsorption at the surface of the catalyst. When the temperature reaches the carbon solubility boundary of the metal, the decomposed carbon particles precipitate and crystallize forming CNTs. The decomposition of hydrocarbons is an exothermic process and carbon crystallization is an endothermic process[33].

Finally, these carbon atoms form nanomaterials depending on the shape and size of the catalysts. The CVD process is known as thermal CVD in the case where hydrocarbon

is decomposed using only heat[31]. The addition of metal, the catalyst–substrate interaction, carbon source and temperature affect the quality and yield of the carbon nanotubes in the CVD process. Water vapor along with carbon sources has also been used to produce clean and super-grown carbon nanotubes[28].

Transition metals are commonly used to achieve a higher carbon production in the CVD process. The stronger metal-support interaction also leads to the growth of filamentary carbons with narrower diameters. Bimetallic Ni-Fe catalysts showed greater C-C cleavage and cracking activity. The type of metal, metal-support interaction and carbon solubility influence the characteristics of the carbons. If this interaction is very weak, it can cause sintering of the metal catalyst. However, if a very strong interaction occurs, the yield of the CNT is low and the materials have low quality. In general, mixed metal catalysts perform better than single metal catalysts[15], as can be seen in Table 2.

Table 2 summarizes the most relevant studies related to pyrolysis of plastic and its catalysts by CVD process, respectively. Noticing that ferrocene ($C_{10}H_{10}Fe$) can decompose and release Fe as catalyst, MA-PP means malleated polypropylene and Ni commercial catalyst is a metallic phase of Ni, supported on Al_2O_3 and doped with Ca, with NiO content being 14%. Most of the catalysts are metals but many of them were commercial catalysts, and the temperatures are in the literature range.

Bajad et al, 2017[34] studied plastic pyrolytic gases for the synthesis of CNTs and enhanced hydrogen recovery during the process, and come to many conclusions such as that the higher amount of hydrocarbon gases results in more conversion to CNTs, while the increased concentration of H_2 was reported due to the separation of carbon from hydrogen during the adsorption of carbon onto the catalyst. Zhuo et al, 2010[35] reviewed the pyrolysis process followed by premixed combustion, the resulting gaseous pyrolyzates generate agents for CNT growth on catalytic surfaces. Tripathi et al, 2017[36] used a stainless-steel CVD furnace as the catalyst to promote the CVD process in PP to MWCNTs, using ranges of temperature form 600 to 1100 °C. The co-production of hydrogen and carbon nanotubes from catalytic pyrolysis of waste plastics on a Ni-Fe bimetallic catalyst showed that a maximum H_2 yield of 8.47 g g^{-1} plastic, and H_2 content of 73.93 vol.% were obtained with the NiFe13 catalyst having the highest fraction of Fe[37]. Although, the presence of Ni enhanced the thermal stability of the CNTs with less carbon

defects, a higher graphitization degree of carbon, and higher thermal stability of filamentous carbon over the NiFe13 catalyst was obtained[37].

Table 2. CNT production from PSWs by CVD

Carbon source	Catalyst	Main results	Temperature	Reference
67.2% HDPE+11.2% PP+6.2% PS+5.2% PVC+10.2% PET	Ni/Mo/MgO catalysts with molar ratio 4:0.2:1	MWNTs	500 to 900 °C	Bajad et al, 2017[34]
PE+MA-PP	$C_{10}H_{10}Fe$	The yield of CNTs was over 80% including about 5% helical CNTs	700 °C	Kong et al, 2007[38]
HDPE	Ni commercial catalyst	An increase in temperature from 600 to 700 °C enhances reforming reactions, and conversion of 98.1%	600 to 700 °C	Barbarias et al, 2018[39]
PP+MA-PP	Ni	MWCNTs diameters in the range of 50-60 nm	830 °C	Jiang et al, 2007[40]
PP+PE	Ni/Al_2O_3	Lower quality CNTs compared to the waste plastics gasification pilot-scale system	750 °C	Yang et al, 2015[41]
40% HPDE+35% LDPE+20% PP+5% PS	Ni-Fe based zeolite catalysts	MWNTs diameters in the range of 12 - 25 nm.	800 °C	Yao et al, 2021[42]
HDPE and LDP	Stainless steel type 304 with Cobal, Ni	MWNTs diameters in the range of 30–85 nm	800 °C	Zhuo et al, 2010[35]
58.6% PE+26.9% PP+ 5.6% PET+8.8% PS+ 0.1% thermoset	$Cu/CaCO_3$	MWNTs were majorly filamentous type	800 °C	Singh et al, 2020[18]
40% HPDE+35% LDPE+20% PP+5% PS	NiFe13, NiFe12, NiFe11, NiFe21, NiFe3	CNTs with narrower diameters were grown with higher Ni ratio.	800 °C	Yao et al, 2018[43]
PP	Ni/SiO_2 and Fe/SiO_2	The Fe-based catalyst with the largest metal particles resulted in the highest yield of carbon (29 wt.%).	800 °C	Liu et al, 2017[44]
PP	SS316 tube (high content of Fe and Ni)	900 °C the highest yield of MWCNTs	600 to 11000 °C	Tripathi et al, 2017[36]
PP, PE and PVC	$C_{10}H_{10}Fe$	Growth rate of CNT arrays is about 12 μm/min	850 °C	Yang et al, 2010[45]
HDPE	Ni/ZSM5, Ni/β-zeolite-2 and Ni/Y-zeolite-3	Significant carbon (~6 wt.%) were observed on the reacted Ni/Y-zeolite-3 catalyst which accounted	850 °C	Chen et al, 2018[46]

for the lower catalyst activity.

2.4.1 The growing process

The growth of the nanotubes by the catalytic CVD method always proceed with the carbon source being decomposed onto the catalyst, and after the atomic carbons diffuse and form a graphitic tubular structure around the particles[47]. The carbon sources can be in solid, liquid or gaseous forms[30]. For the interaction between the catalyst and the substrate, there are two growth mechanisms, as represented in Figure 8 and in Figure 9.

In the early stage of CNT nucleation, the first cross-linked carbon chains formed on the surface of the large catalyst can quickly diffuse to the catalyst/substrate interface and stabilize it (step 2). This step leaves the upper surface of the nanoparticle exposed for greater carbon absorption, almost an excess, leading to particle elongation at the top of the CNTs (step 3) and finally drives the particle lift-off from the substrate, a weak iteration[33] (step 4). Once the connection with the substrate is broken, the growth follows a "tip-growth" mechanism[47].

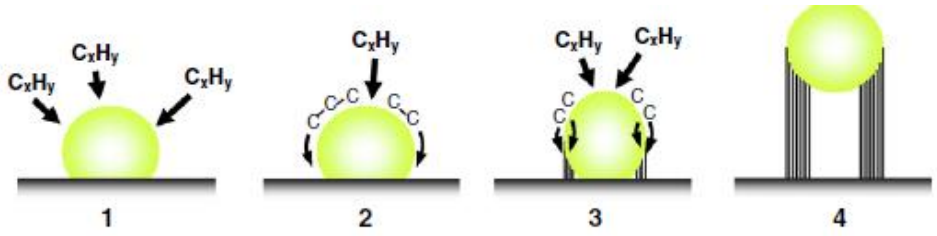

Figure 8. Tip-growth mechanism diagrams for CNT. Source: Gohier A. et al, 2008 [47]. Image reproduced with permission of the rights holder, Elsevier.

In the case of the small metal particles, assuming a much more reactive metal particle, this implies a stronger interaction with the carbon patch. Hence, after dehydrogenation of the first molecules of C_xH_y, a graphene cap is formed (step 2) and cuts off the carbon source over the particles (step 3). Therefore, the carbon flux can only be provided at the nearby interface between the catalyst and the substrate[47]. Thus it is forced to precipitate from the top of the metal, called the "base-growth"[33] (step 4).

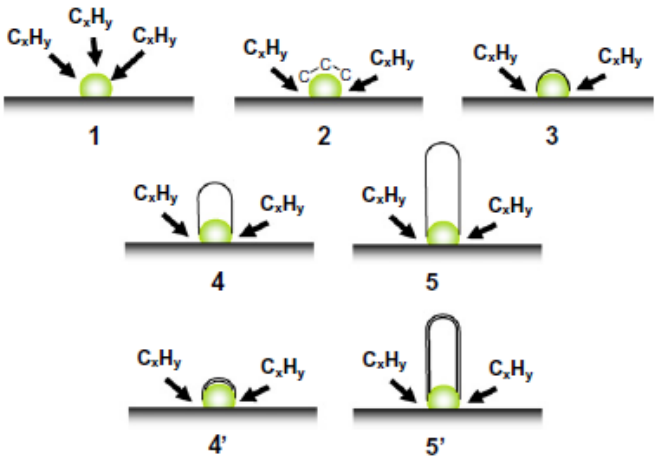

Figure 9. Base-growth mechanism diagrams for CNT. Source: Gohier A. et al, 2008[47]. Image reproduced with permission of the rights holder, Elsevier.

The behavior of "tip-growth" occur only for the large MWCNT, while the "base-growth" mechanism is observed on SWCNT[47].

According to Rajesh Purohit et al, 2014[29], there are many growth parameters involved in the synthesis of CNTs, as catalyst concentration, catalyst particle size, pressure, growth time, growth temperature and gas flow rate. So, particle size is not the only condition that controls the growth mechanism but it is one of the conditions for choosing tip- or base-growth[47]. But also, other parameters affect the final morphology and yield of CNTs, such as carbon source, reactor temperature, system pressure, deposition time, reactor type, the geometry of reactor and active metal components in a catalyst.

There are various techniques used for the growth of CNTs. The most popular methods are arc discharge, laser ablation and CVD. Both techniques providing energy to a carbon source for the creation of carbon atoms that result in CNTs[29]. Comparing these methods, one of the advantages of CVD methods is that they have more control over the morphology and structure of the produced nanotubes[33]. Being able to produce individual nanotubes well separated or supported on flat substrates or suspended in trenches[41]. CVD is superior to arc and laser methods in terms of yield and purity.

2.4.2 Catalysts

In a pyrolysis process, the use of a catalyst allows decreasing the temperature and the retention time, requiring less energy and optimizing the process. The catalyst acts by changing the mechanism of the chemical reaction, decreasing the activation energy.

In the synthesis of CNTs by CVD, the catalyst deposited substrate and the nucleation catalyst are carried. The catalyst particle can stay at the bottom or top of the growing carbon nanotube, this particle determines the nanoscale curvature of the CNTs[31]. Specific carbon nanotube synthesis requires different catalysts. It is the carbon source decomposition active center and graphite carbon deposition center in the growth process of CNTs. The influence of the selection, preparation and carrier selection of CNTs can change the morphology and structure, in scenarios as nucleation, growth rate, density, separation and purification[33].

The most commonly used metals are Fe, Co and Ni[48], due to the high solubility of carbon in these metals at high temperatures; and the high carbon diffusion rate in these metals, nucleation and growth of carbon atoms can be carried out[33]. Besides that, the high melting point and low equilibrium-vapor pressure of these metals can result in a wide temperature window of CVD for a wide range of carbon precursors[27]. These parameters provide a wide range of temperatures for various carbon sources and can be used to grow carbon nanotubes at different temperatures.

Other metals can be used to catalyze hydrocarbons for growth of CNTs, such as Cu, Au, Ag, Pt and Pd[27]. Solid organometallocenes, as ferrocene, cobaltocene and nickelocene are also widely used as a CNT catalyst because they liberate metal nanoparticles in-situ, catalyzing the hydrocarbon decomposition more efficiently. Alumina materials are reported to be better catalyst support than silica owing to the strong metal–support interaction in the former, which allows high metal dispersion and thus a high density of catalytic sites[27].

Both catalytic reactivity and energy consumption are always suggested for bimetallic catalysts by integrating different materials. Some bimetallic catalysts like Ni-Mg, Ni-Mn and Fe-Ru have been studied for the filamentous carbon production from pyrolysis-catalysis of polymers[37]. The advantages of those bimetallic or trimetallic catalysts are good stability, smaller metal particle size and appropriate interaction or synergy between metals[37].

2.4.3 Iron catalysts

Iron catalysts with high melting points are more suitable for high temperature reactions than Ni catalysts. For the use of Fe_2O_3 of the nanoscale particles, it is made by its fundamental magnetic characteristics. To improve the mechanical side of Fe_2O_3

without changing its magnetic properties, Al_2O_3 has been used lately due to its properties such as high insulation, high hardness, high stability and transparency[49]. From an economic perspective, the transition metal oxide, such as iron oxide and Fe_2O_3/Al_2O_3[50] is also cheaper than common Ni and Co catalysts.

Magnetite (Fe_3O_4) nanoparticles have magnetic properties on the morphologies of nanoparticles. When the size of these nanoparticles is very small, the size of single magnetic domain is equal to that of each particle. In the study of Shi et al, 2010[51] for controlling the size and size distribution of magnetite nanoparticles on carbon nanotubes, showed that Fe_3O_4/CNTs nanocomposites had superparamagnetic characteristics.

According to Liu et al, 2019[50], comparing with iron oxide catalyst, the stability of Fe_2O_3/Al_2O_3 catalyst is significantly improved. And when the reaction continues, the conversion rate of hydrogen decreased slowly.

A simple and efficient method for synthesizing Fe_2O_3/Al_2O_3 is the sol-gel method, producing a number of metal oxide nanoparticles with high purity, high surface area, good uniformity and low processing temperatures[49].

The starting material for sol-gel preparation typically uses either colloidal dispersions or inorganic precursors. The synthesis involves a colloidal suspension of solid particles in a liquid, called sol, and subsequent formation of a double-phase material from a solid body occupied with a solvent, the gel. This method can achieve very high purity due to the quality of available precursors[52].

2.4.4 Flow rate

The flow rate of the carrier gas is also an influential parameter on the growth of CNTs, verified by S. Porro et al, 2007[53], to allow the growth of fine nanotubes, there should probably be a low concentration of catalyst and a high flow of carrier gas. Although the flow of nitrogen gas and the concentration of the catalyst cannot be considered independently of each other and also from temperature, they have shown a side effect on the diameter of the CNT.

Malgas et al, 2008[54] have grown vertically aligned CNTs using CVD on a silicon substrate by using an inexpensive carbon source. Indicated for higher degree of graphitization, the higher nitrogen carrier gas flow rates should be used. The final results

showed that diameter, density and growth rate of MWCNTs can be controlled by adjusting the mixture ratios and nitrogen carrier gas flow rates[54].

Although the investigation about the effects of the type of carrier gas and the carrier gas flow rate on the formation of CNTs[55], using pyrolyzate gases of waste polyethylene feedstocks, showed that the most favorable gas at the slowest flow rate is nitrogen, and was somewhat influential on the nominal lengths of the CNTs.

2.4.5 Temperature

According to Yang et al, 2003[30], the optimal synthesis temperature is closely related to the nature of the feeding gas. The usual temperature ranges for the CVD process are 600 to 1200°C. S. Porro et al, 2007[53], after the analyzed growth parameters, for controlling the CNT diameter the growth temperature is the most influential. Their research said that a not good environment for CNT growth is when the concurrent employment of a low feeding gas flow, a low catalyst concentration and a rather low temperature[53].

Aboul-Enein et al, 2017[56] converted LDPE to carbon nanotubes in a two-stage process (pyrolysis-decomposition). The conclusion was that the yield of gases fraction produced at different pyrolysis temperatures influences on the yield of CNTs and, the quality and yield of the produced CNTs are significantly influenced by the decomposition temperature of the pyrolysis gases.

At higher temperatures, an increased supply of pyrolysis gases causes excessive carbon feeding, leading to catalyst poisoning. At the same time, agglomeration of a metal particle at high temperature leads to the growth of CNTs with large diameters[15]. Also, results in higher graphitization degrees and higher yield of CNTs than at low temperature[33]. Carbons of different morphology can be observed at different temperatures. Finding a way to grow CNTs at room temperature is a big challenge. At lower temperatures, there is an incomplete conversion of hydrocarbons that leads to a lower gas production[15].

The reason why MWCNTs are easier to grow (than SWCNTs) from most of the hydrocarbons, is due to the CVD low-temperature (600–900 °C) yields the particle, and the precursors (viz. acetylene, benzene, etc.) are unstable at higher temperature. While SWCNTs grow from selected hydrocarbons (viz. carbon monoxide, methane, etc.),

whereas high-temperature (900–1200 °C) reaction favors SWCNT growth. This indicates that SWCNTs have higher energy of formation (presumably owing to small diameters; high curvature bears high strain energy)[57].

3 Objectives

The overall aim of this MSc thesis is to study the process of valorization of plastic solid waste into CNTs by sequential pyrolysis of the plastics, in which several volatile organic compounds are produced, and the CCVD of those volatile organic compounds produced on the metallic materials, where growth of CNTs occurs.

3.1 Specific aims

- Preparation of magnetic nanoparticles by sol-gel to be used as catalysts in CVD.
- Preparation of carbon nanostructures by CVD with the catalytic nanoparticles previously prepared.
- Evaluation of the time, temperature and of the nitrogen flow effects on the yield of CNTs.
- The study of pyrolysis of waste plastics, using pure polyolefins representative of plastic solid wastes. The kinetics of plastics conversion (LDPE, HDPE, PP and MIX) will be evaluated considering different times and nitrogen flow rates at a temperature of 600 ºC.
- Characterization of magnetic nanoparticles and CNTs by XRD, FT-IR, titration to acidity and basicity, surface area analysis and ash content.

4 Methodology

4.1 Reactants

The reactants used in this work are described below, according to the application for which they were used.

Production of catalysts:

- Aluminum oxide, BASF. Formula: Al_2O_3;
- Ethanol Absolute (99.99%), Fisher Chemical. Formula: C_2H_5OH;
- Ethylene glycol (99%), Fisher Chemical. Formula: $C_2H_6O_2$;
- Iron (II) chloride tetrahydrate, Acros Organics. Formula: $FeCl_2 \cdot 4H_2O$;
- Iron (III) chloride hexahydrate, VWR Chemicals. Formula: $FeCl_3 \cdot 6H_2O$.

Carbon nanotubes synthesis and washing:

- High-density polyethylene (HDPE), melt index 2.2 g/10 min, Sigma-Aldrich. Formula: $[C_2H_4]_n$;
- Low-density polyethylene (LDPE), weight average molecular weight ~35,000, number average molecular weight ~7,700, Sigma-Aldrich. Formula: $[C_2H_4]_n$;
- Polypropylene (PP), weight average molecular weight ~250,000, number average molecular weight ~67,000, Sigma-Aldrich. Formula: $[C_3H_6]_n$;
- Sulfuric acid (95%), VWR Chemicals. Formula: H_2SO_4;
- Distilled water.

All reagents were used as received without further purification.

4.2 Preparation of materials

4.2.1 CVD-Catalyst

The catalyst consists of magnetite supported on alumina. To obtain the magnetite prepared by sol-gel method on powdered alumina, 20 mL of ethanol and 10 mmol of $FeCl_2 \cdot 4H_2O$ were stirred and heated in a beaker until the boiling point is reached and then cooled to room temperature. In another 250 mL beaker, 80 mL of glycol ethylene and 20 mmol of $FeCl_3 \cdot 6H_2O$ were stirred and heated at 60 °C for 5 min and then cooled to room temperature. Both previously prepared mixtures and 6.6 g of alumina were added into a beaker, stirred, and heated at 60 °C for 2 h, as shown in Figure 10 a). The system was

heated at 120 °C until the gel texture was achieved. At last, the gel was heated at 200 °C until the dry powder formed, being cooled to room temperature at the end, as shown in Figure 10 b). For discussion, this material is called “Catalyst_before”.

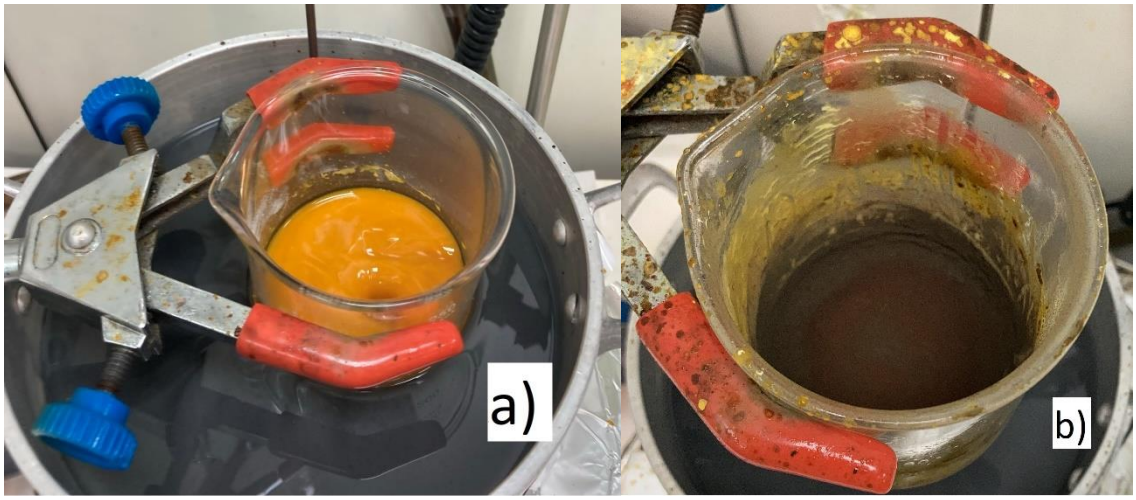

Figure 10. a) Catalyst at 60 °C. b) Catalyst at 200 °C.

The powder synthesized in the previous step was submitted to heat treatment. The catalyst was calcined at 300 °C for 12 h and at 600 °C for 24 h with a 0.1 L/min of nitrogen flow. After the heat treatment, the material is called “Catalyst_after”.

4.2.2 Production of CNTs

The furnace used to produce CNTs is a tubular oven with 50 mm of internal diameter and 500 mm long, disposed in a vertical position and designed by TERMOLAB, represented in Figure 11.

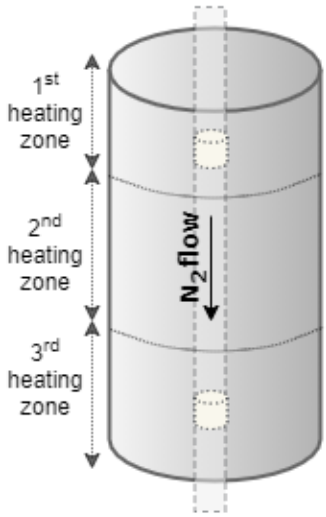

Figure 11. Experimental set up used in the synthesis of CNTs by CVD.

In a typical experiment, 5 g of pure polymer and 1 g of catalyst were placed in the crucibles located at the top and bottom heating zones, respectively, the crucibles observed in Figure 12 a). For the run conducted with a mixture of polymers: 1.75, 1.25, and 2 g of LDPE, HDPE and PP were used, respectively. The crucibles were placed in the tubular furnace under a nitrogen flow of 10, 20 or 40 mL/min for 2 h. In this inert atmosphere, the test was conducted at the temperatures of 600, 700 or 800 °C. At the end of the process, the crucible containing the catalyst and the polymer will remain in the tubular furnace until reaches ambient temperature, and the result is shown in Figure 12 b).

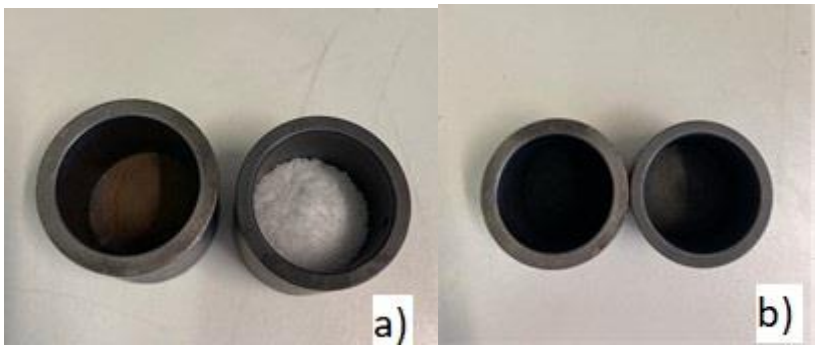

Figure 12. a) Before: left crucible contains catalyst and right crucible a polymer. b) After: left crucible contains CNT and right crucible is empty.

To evaluate how efficient was the process, the yield was calculated taking in account the amount of carbon present in the carbon source (polymer) and the carbon present in the structure of the CNTs, determined by an ash content test described below, using Equation 1.

$$Yield = \frac{\text{total mass} - \text{catalyst mass}}{\text{catalyst mass}} x100 \quad (1)$$

It will be produced two types of CNT, one of retention time and other without retention time. The first will be written as R with 0 min, 30 min and 60 min of retention, as seen in Table 3.

Table 3. Retention materials

Sample	Polymer	Temperature (°C)	Flow (mL/min)	Time (min)
LDPE_600-10-0-R	LDPE	600	10	0
LDPE_600-10-30-R	LDPE	600	10	30

LDPE_600-10-60-R	LDPE	600	10	60

4.2.3 Purification of CNTs

All CNT prepared were purified by washing with sulfuric acid, following the same procedure as described elsewhere[58]. First, in a round-bottom flask, 1 g of CNTs is added to 50 mL of H_2SO_4 (50% vol.). The round-bottom flask is then coupled to a condenser and immersed in a heating bath, being kept under agitation for 3 h at 140 °C. Once at room temperature, the volume of liquid is diluted with distilled water and the contents are filtered. The material is washed thoroughly with distilled water until the rinsing waters reaches neutral pH. The purified CNT are finally taken to the oven to dry overnight at 60 °C.

4.2.4 List of materials

Table 4 summarizes the different purified CNT prepared in this work, with its respective polymer and conditions of synthesis. Without retention time.

Table 4. Purified materials

Sample	Polymer	Temperature (°C)	Flow (mL/min)
P-LDPE_600-10	LDPE	600	10
P-LDPE_700-10	LDPE	700	10
P-LDPE_800-10	LDPE	800	10
P-LDPE_600-25	LDPE	600	25
P-LDPE_700-25	LDPE	700	25
P-LDPE_800-25	LDPE	800	25
P-LDPE_600-40	LDPE	600	40
P-LDPE_700-40	LDPE	700	40
P-LDPE_800-40	LDPE	800	40
P-HDPE_800-40	HDPE	800	40

P-PP_800-40	PP	800	40
P-MIX_800-40	MIX	800	40

4.3 Characterization of materials

The CVD-catalyst and the unpurified and purified CNTs were characterized by Fourier Transform Infra-Red spectroscopy (FT-IR), analysis of ash content, acid-based characterization, porosimetry and X-ray diffraction (XRD), as described in the following sub-sections.

4.3.1 FT-IR analysis

Fourier Transform Infrared Spectroscopy (FT:IR) is a technique used to observe the bands related to vibrations of bonds or atoms present in a sample[59]. The FT-IR spectra of the 12 different CNTs (see Table 4) and of 2 catalysts (before and after heat treatment), were recorded on a Perkin Elmer FT-IR spectrophotometer UATR Two infrared spectrophotometer, with a resolution of 4 cm^{-1}. The range of wavenumbers used in the analysis was from 400 to 4000 cm^{-1}. All measurements were done with the solid samples at room temperature. This analysis was performed at the Analytical Chemistry Laboratory of the Bragança Polytechnic Institute (IPB).

4.3.2 Analysis of ash content

The methodology used to evaluate the ash percentage of the materials was adapted from J. Cardoso et al, 2019[60]. It consists in the oxidation of all organic matter in a weighed sample of the material by incineration and determining the weight of the remaining ashes. The materials (CVD-catalyst and unpurified and purified CNTs), in duplicate, were burnt in a muffle at 450 °C until a constant mass was reached in a precision balance (±0.0005 g). For this evaluation, the percentage of organic and catalyst fractions was considered, since the materials are composed of a carbonaceous (CNTs) and of an inorganic structure (CVD-catalysts used for the growth of the CNTs).

4.3.3 Acid-base characterization

The acidity and basicity of the samples (CNTs after purification) were determined following methodologies described by Silva et al, 2019[61]. Those properties were determined by titrating a solution of NaOH and HCl after being in contact with the solid materials during 48 h. For that purpose, 0.1 g of solid sample was added in 2 different

erlenmeyers. One of the erlenmeyers contained 10 mL of a 0.02 M HCl solution for basicity determination, and the other 10 mL of a 0.02 M NaOH solution for acidity determination. The resulting suspensions in the erlenmeyers were placed in an orbital shaker IKA KS 130 Basic and stirred for 48 h at 200 rpm. After stirring, the suspension of each erlenmeyer was filtered to remove the solid material, and 5 mL was used for the determination of the concentration by titration. Phenolphthalein was used as an indicator in both titrations. For titration, 0.01 M HCl was used to determine the acidity. For the basicity it was used 0.01 M NaOH.

4.3.4 Porosimetry

The textural properties of the materials were determined by analysis of N_2 adsorption–desorption isotherms at 77 K, obtained in a Quantachrome NOVATOUCH XL[4] adsorption analyser. The degasification of the materials was conducted at 120 °C during 16 h and then BET (S_{BET}), Langmuir specific surface area ($S_{Langmuir}$) were determined using BET and Langmuir methods, respectively. The total pore volume (V_{Total}) was determined at $p/p^0 = 0.98$. The calculations were done using TouchWin™ software v1.21. Briefly, BET and Langmuir equations (Eq.(2) and Eq.(3)) were applied to determine the volume adsorbed in the monolayer parameter (n_m), according to those methods:

$$\frac{p/p^0}{n(1-p/p^0)} = \frac{1}{n_m C} + \frac{C-1}{n_m C}(p/p^0) \tag{2}$$

$$\frac{p/p^0}{n} = \frac{1}{C.n_m} + \frac{p/p^0}{n_m} \tag{3}$$

Where p/p^0 is the relative pressure, n is the specific amount adsorbed at the relative p/p^0, n_m is the specific monolayer capacity for each method and C is a parameter. Then, BET and Langmuir specific surface areas were determined using the previous n_m determined from each method by Eq. (4)

$$S(m^2\ g^{-1}) = \frac{n_m(m^3\ g^{-1}) \cdot N_A(mol^{-1}) \cdot \sigma_m(m^2)}{V(m^3\ mol^{-1})} \tag{4}$$

Where N_A is the Avogadro's number ($6.03 \cdot 10^{23}$ mol^{-1}), σ_m is the molecular cross-sectional area of N_2 (0.162 nm^2) and V is the molar volume of N_2 (0.023 m^3 mol^{-1}).

The total pore volume (V_{Total}) was calculated using Eq. (5).

$$V_{Total} = \frac{n\left(\frac{p}{p^0} = 0.98\right) \cdot M_{N_2}}{V.\rho} \quad (5)$$

Where M_{N_2} is the molar mass of nitrogen (28.0134 mol g^{-1}), V is the specific volume (0.022414 m^3 mol^{-1}) and ρ its density (0.81 g cm^{-3}).

4.3.5 XRD analysis

To identify the type of metallic particle in the iron catalyst, the measurements of powder XRD were obtained by depositing the material in a glass sample holder and analysing it on a diffractometer DRON-3. The XRD pattern is the fingerprint of periodic atomic arrangements in a given material[62]. For the interpretation of the results, the software HighScore Demo was used, from PANanalytical.

5 Results and discussion

The synthesized materials, CVD-catalyst and CNTs, were firstly analyzed in terms of production yields and after regarding their morphological structures (section 5.4).

5.1 Yield of CVD-catalyst

Under inert atmosphere, 25.1% of experimental yield was obtained, as shown in ANNEXES 7.4.

5.2 Effect of inlet N_2 flow in heating rate of the tubular furnace

The effect of the nitrogen flow in the heating rate of the furnace was evaluated without any material in two zones: the superior zone (or first zone) and the inferior zone (or third zone), represented in Figure 11. In the first case, the superior zone was set to 400 ºC, and the inferior zone to 600 °C with a flow of 10 mL/min, 25 mL/min and 40 mL/min. The results obtained with a N_2 flow of 10 mL/min are shown in Figure 13. The results obtained with higher flows are shown in ANNEXES.

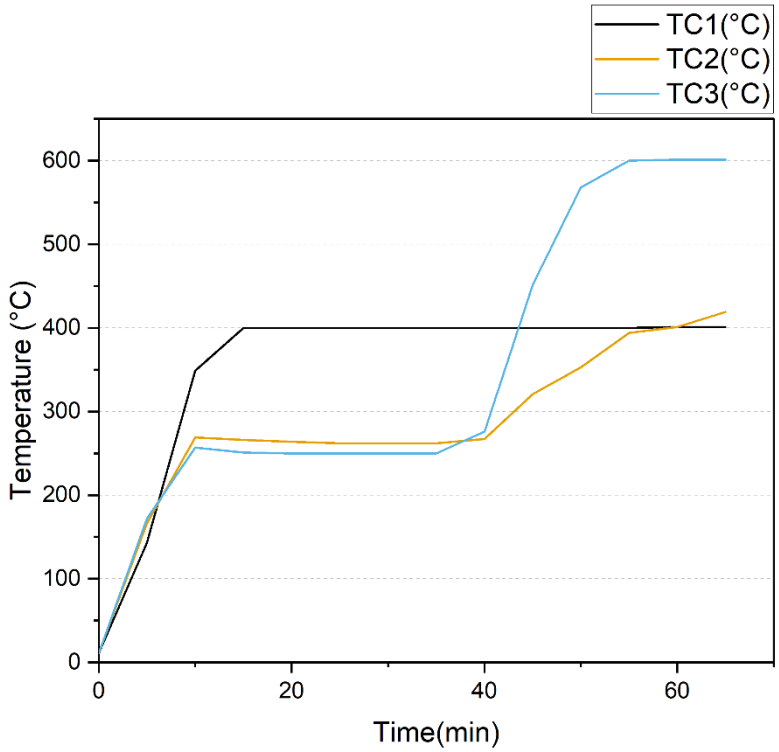

Figure 13. Effect of N_2 flow (10 mL/min) in the heating rate of the superior zone (set at 400 °C) and in the inferior zone (set at 600 °C)

From the results obtained it was found that, irrespectively of the N_2 flow used, the behavior is the same and the set points stabilized after 60 min. It was clear that the first and second zone stabilized at 400°C, but only the first was set up. In a second study, just the inferior zone was set at 600 °C with a flow of 10 mL/min, 25 mL/min and 40 mL/min. The results obtained with a N_2 flow of 10 mL/min are shown in Figure 14. The results obtained with higher flows are shown in ANNEXES.

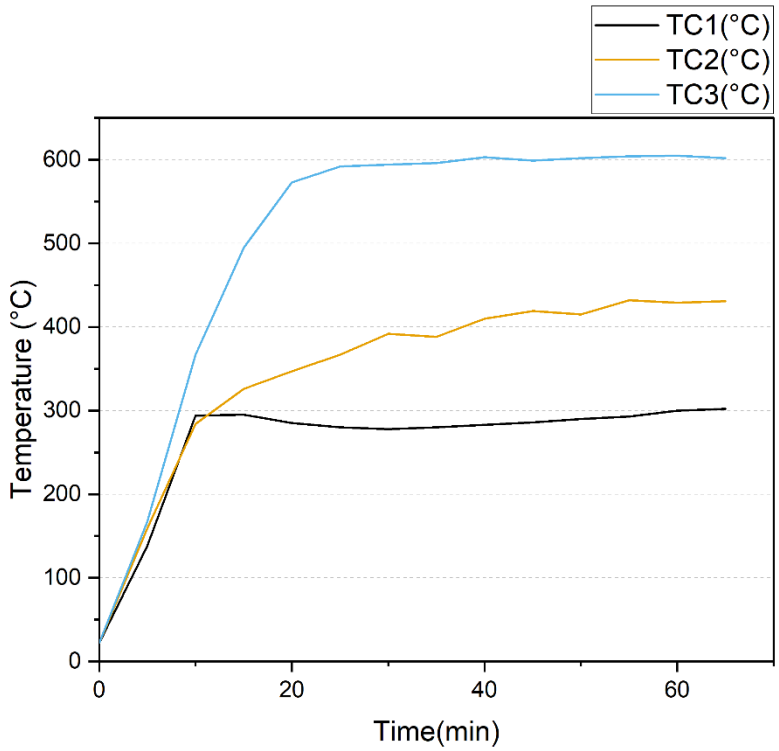

Figure 14. Effect of N_2 flow (10 mL/min) in the heating rate of inferior zone (set at 600 °C)

From the results obtained it was found that, irrespectively of the N_2 flow used, the behavior is the same and the set points stabilized in 60 min too. In this case the second zone stabilized approximately at 430 °C and the first zone at 300 °C. In summary, without any material in the furnace, it was found that the flow does not influence the stabilization of temperature, and that for this 60 min are needed to reach the setpoints. After reaching the set point, this time will be used in the synthesis of CNTs, see section 5.3.2.

5.3 Yields of CNT-growth

5.3.1 Effect of retention time

The effect of the retention time was firstly assessed using LDPE as polymer, controlling the temperature of the furnace system to reach 600 °C at 10 °C/min.

In each experiment N_2 was feed with a flow of 10 mL/min, considering 5 g LDPE and 1 g catalyst. The experiment LDPE_600-10-0-R was only run until temperature reaches 600 °C. The second experiment, LDPE_600-10-30-R, after reaching 600 ºC, the temperature is held for 30 minutes. LDPE_600-10-60-R was the same, but temperature stays 60 minutes after reaching the set point at 600 ºC, shown in ANNEXES Figure 25.

Table 5 represent the results of the experiments in terms of yield of CNTs obtained. The value of yield reflects the comparison between the CNT mass and the polymer mass. The time was a key factor to produce CNTs between these three experiments, as we can see in LDPE_600-10-30-R and LDPE_600-10-60-R. The constant period of 30 and 60 min improves the CVD process. Allowing more time at a constant temperature, the final mass of the produced CNTs was increased.

Table 5.Yield results as a function of retention time upon heating the oven until 600 ºC at 10 °C/min with LDPE.

Sample	Yield (%)
LDPE_600-10-0-R	0.3
LDPE_600-10-30-R	3.7
LDPE_600-10-60-R	3.7
LDPE_600-10	5.1

The CNTs LDPE_600-10-0-R presented a low yield, slightly higher values obtained with LDPE_600-10-30-R and LDPE_600-10-60-R for this reason, they were not purified. The sample LDPE_600-10, CNTs synthesized without time of retention, presents a slightly higher value by the reason to not have a retention, see in section 5.3.2.

Dealing with petroleum derivatives, even though working in an inert atmosphere, some residues are formed. The visible one is wax, probably formed because of the low increase of the temperature, so the material was melted and attach on the stem before subjected to CVD. During the period that the furnace cools down, this melted material turns into solid, forming a wax. The formation of this can be seen at the inferior zone, most precisely, at the end of the stem, as shown in ANNEXES.

5.3.2 Effect of N_2 inlet flow and temperature

The effect of N_2 inlet flow on CNTs yield was studied considering 10, 25 and 40 mL/min. Without retention time and, regarding the effect of temperature the first zone of the oven was maintained in all experiments at 400 °C, and only the temperature in the

third zone was changed to 600, 700 and 800 °C (see Figure 11 for identification of the zone). The results obtained are gathered in Table 6.

Table 6. Yields of CNTs synthesized from LDPE upon variation of N_2 flow (10, 25 and, 40 mL/min) at 600, 700 and 800 °C.

Sample	Precursor	CNT mass (g)	N_2 Flow (mL/min)	Temperature (°C)	Yield (%)
LDPE_600-10	LDPE	0.2548	10	600	5.1
LDPE_700-10	LDPE	0.4408	10	700	8.8
LDPE_800-10	LDPE	0.5267	10	800	10.5
LDPE_600-25	LDPE	0.2515	25	600	5.0
LDPE_700-25	LDPE	0.3179	25	700	6.4
LDPE_800-25	LDPE	0.7891	25	800	15.8
LDPE_600-40	LDPE	0.2691	40	600	5.4
LDPE_700-40	LDPE	0.34097	40	700	6.8
LDPE_800-40	LDPE	0.8466	40	800	16.9

The presented data show the effect of temperature and N_2 flow on the yield of CNTs obtained from the polymer LDPE upon catalytic CVD, as seen 2.4.4 the nitrogen flow rate is a good choice and, higher temperatures produce different yields (2.4.5). The best results were obtained at 800 °C and 40 mL/min, conditions chosen to study the effect of other polymers on the CNTs production. These parameters have influence in CNT magnetism, LDPE_800-40 had superior magnetism than LDPE_600-40 and LDPE_700-40. An example of this characteristic is shown in Figure 15.

Figure 15. An example of magnetism of the synthetized CNT.

In the experiments carried out for all flows and temperatures, a residue was obtained, an oil with a strong smell, probably the polymer products that did not reacted in the CVD process, which become combustible, as shown in ANNEXES.

5.3.3 Effect of plastic feedstock

Based on the results presented in the previous section, the last configuration conditions were selected for further experiments HDPE, PP and MIX (800 °C and 40 mL/min).

Table 7. Synthesis of CNTs from HDPE, PP and MIX in a usual configuration considering 800 °C and 40 mL/min of N_2 feed.

Sample	Material	CNT mass(g)	Nitrogen flow (mL/min)	Temperature (°C)	Yield (%)
HDPE_800-40	HDPE	0.42722	40	800	8.5
PP_800-40	PP	0.3375	40	800	6.7
MIX_800-40	MIX	0.42768	40	800	8.9

Temperature was found to be fundamental for the increase of yield, but the properties of the polymer was also found to be influencing. Table 7 shows a good yield for HDPE and MIX, 6.7% from PP is also similar to LDPE_700-40. For these reasons, to better understand that influence, the characterization of the materials for LDPE_600-40 (same temperature of catalyst), LDPE_800-40, HDPE_800-40, PP_800-40 and MIX_800-40 will be carried out.

As seen previously in Table 2, Bajad et al, 2017[34] obtained CNTs from mixed polymers at different temperatures, although the time in the furnace was 20-10 min with the exit gases being recycled. The yield results for those nanotubes synthesized at 600 °C were

found to be low, which was attributed to the oxidation of CNTs by a high concentration of CO and CO_2 in the gaseous stream with a higher recycle ratio. In addition, the maximum yield for this study is also obtained at 800 °C.

Other reports reveal that the yield of gas from pyrolysis of PE increases with temperature, accounting only for 5.7 % at 500 °C, and reaching a maximum of 96.5 % at 800 °C, decreasing thereafter with increasing temperature[35]. This effect also occurs with HDPE, an increase in temperature from 600 to 700 °C enhancing reforming reactions and leading to high conversion (98.1%)[39].

5.3.4 Purification

The yields obtained in the purification of the materials are summarized in Table 8.

Table 8. Yields obtained in the purification of the synthesized CNTs.

Sample	Yield (%)
P-LDPE_600-10	38.1
P-LDPE_700-10	25.1
P-LDPE_800-10	49.1
P-LDPE_600-25	31.6
P-LDPE_700-25	32.5
P-LDPE_800-25	52.7
P-LDPE_600-40	54.8
P-LDPE_700-40	34.1
P-LDPE_800-40	45.2
P-HDPE_800-40	38.4
P-PP_800-40	41.6
P-MIX_800-40	46.1

From analysis of Table 8 it is observed that the materials synthesized at 800 °C are those presenting the highest percentage of purified material. The materials synthesized with a nitrogen flow of 40 mL/min also presents higher values. The interesting fact is that LDPE_600-40 also presents significant data for this analysis.

The purification with sulfuric acid is efficient to remove impurities and some organic content, the maximum percentage purification yield values also being obtained for the materials synthesized in the same conditions that gave higher synthesis yield (800 °C and 40 mL/min of N_2 flow). The Analysis of ash content obtained before and after the purification allows for better interpretation of the results, in Table 10.

5.4 Characterization of Materials

5.4.1 Textural properties

Figure 16 presents the isotherms of the purified CNT materials and of the catalyst after heat treatment. The S_{BET} and V_{pore} values are summarized in Table 9.

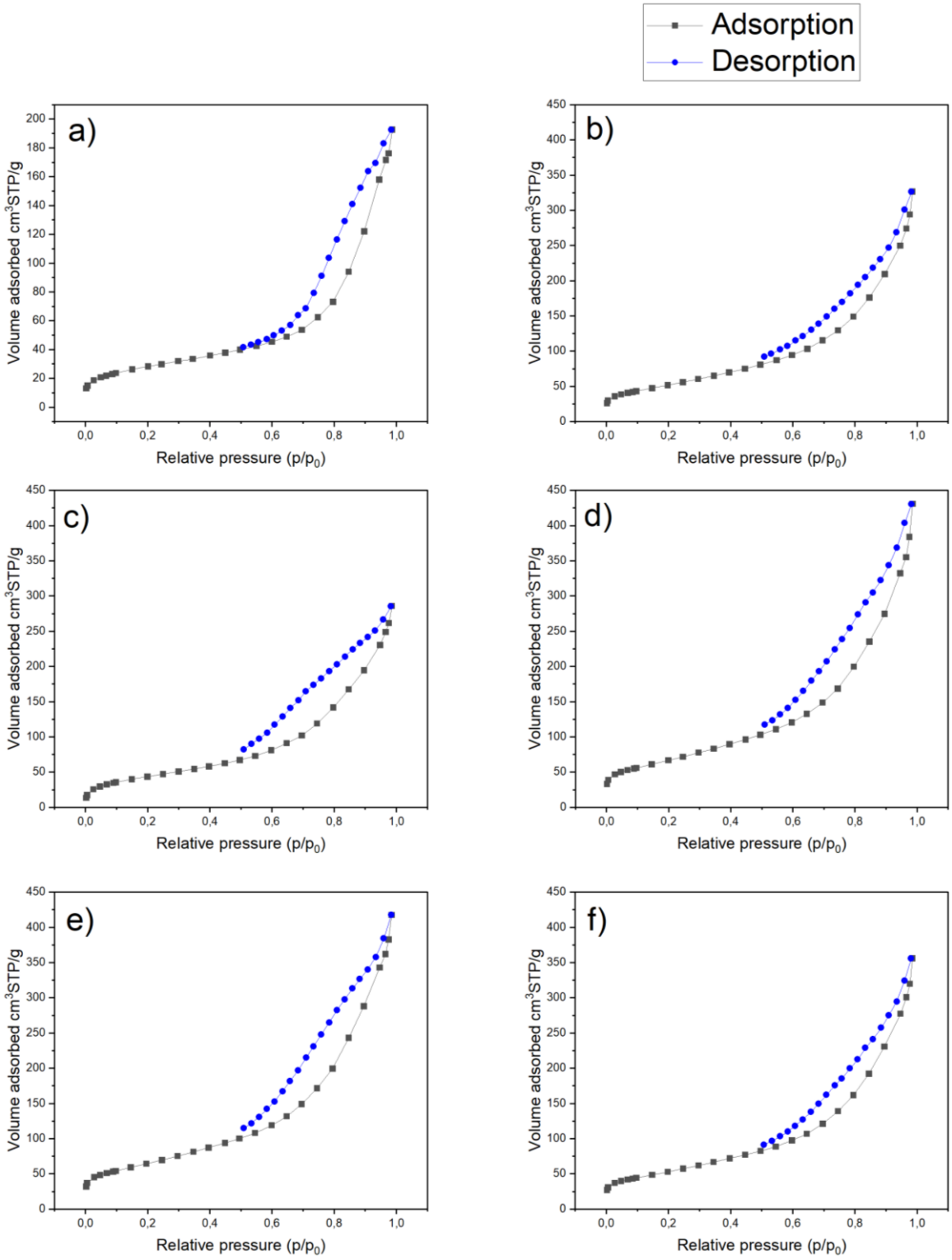

Figure 16. Isotherms of adsorption −desorption of a) Catalyst_after, b) P-HDPE_800-40, c) P-LDPE_600-40, d) P-PP_800-40, e) P-LDPE_800-40 and f) P-MIX_800-40.

As can be observed, all CNTs (b, c, d, e and f) have similar behavior. According to IUPAC[63], these types of isotherms are characteristic of type II, monolayer-multilayer adsorption with a hysteresis loop of type-H4, classified as micro-mesoporous carbons.

The catalyst exhibited a type-IV isotherm with a distinct hysteresis loop of type-H3[63]. The adsorption hysteresis is also classified in the mesoporous type, this behavior being found in the analysis of a similar catalyst (Fe_3O_4@PPy NPs.) prepared by Tavousi et al, 2020[64] and Liu et al, 2015[65].

Table 9. BET surface area and pore volume of the purified materials and of the CVD-catalyst after heat treatment.

Sample	S_{BET} (m^2/g)	$S_{langmuir}$ (m^2/g)	V_{total} (cm^3/g)
P-LDPE_600-40	159	180	0.406
P-LDPE_800-40	235	257	0.594
P-HDPE_800-40	189	203	0.456
P-PP_800-40	242	265	0.595
P-MIX_800-40	194	209	0.496
Catalyst_after	98	114	0.273

All CNTs presented reasonable values of S_{BET} between 159-242 m^2/g, only the catalyst presented a low value, this repeats in the volume. In the CVD process, the interaction between catalyst and polymer improves the surface area.

Some examples of specific surface areas reported for CNTs are 80.9 m^2/g [66], 90.2 m^2/g[67] and 71.24 m^2/g[68], but in open literature generally have the range of 100–300 m^2/g.[69] According to Peigney et al, 2001[70], in their theoretical study about surface area calculation, the theoretical specific surface area range over a very broad scale, from 50 to 1315 m^2/g and this value depends on the number of walls.

The high values found for CNTs match with the study from Martin-Martinez et al, 2019[71], corresponding to high purity materials. Also, upon modification by treatment by immersion in dilute acid, reported by Zhang et al, 2005[72], it was described that these increase in the values are due to the internal surface area that could be effectively used, leading to the increase of the specific surface area and pore volume. These values are noticed in Table 8 for the purified materials, in which the same samples present less ash content after acid washing, which may increase the surface area in these materials.

For the pore volumes of the CNTs, the results obtained are similar to the reported in literature[72,73]. For the catalyst, a study for the preparation of CNT using Fe@Al_2O_3 core–

shell nanocomposites demonstrate that the catalyst has a BET surface area of 89.37 m^2/g[74]. And, for catalyst pore volume, the value is in the literature range[5,42].

5.4.2 XRD

The phase purity and crystallinity of the CVD-catalyst was studied by XRD analysis, and the pattern is shown in Figure 17. XRD pattern of the CVD-catalyst synthesized under inert atmosphere upon calcination at 300 °C for 12 h and at 600 °C for 24 h. The material, synthesized under inert atmosphere upon calcination at 300 °C for 12 h and at 600 °C for 24 h, contained corundum ($\alpha - Al_2O_3$) and hematite (Fe_2O_3).

The crystal structure of Fe_2O_3 is a rhombohedral α-Fe_2O_3 with lattice parameters a = b = 5.0356 Å and c = 13.7489 Å. The values match precisely with the standard data (JCPDS Card No. 34-0664). The hematite phase, corresponding to crystal planes (012) (104) (110) (113), (024), (116), and (300) is similar that obtained in the work of Khodadadi et al, 2019[75]. Sharp peaks for each crystal plane are observe at the 2θ angles of 24.26°, 33.26°, 35.79°, 40.98°, 49.60°, 54.17°, and 64.10° respectively.

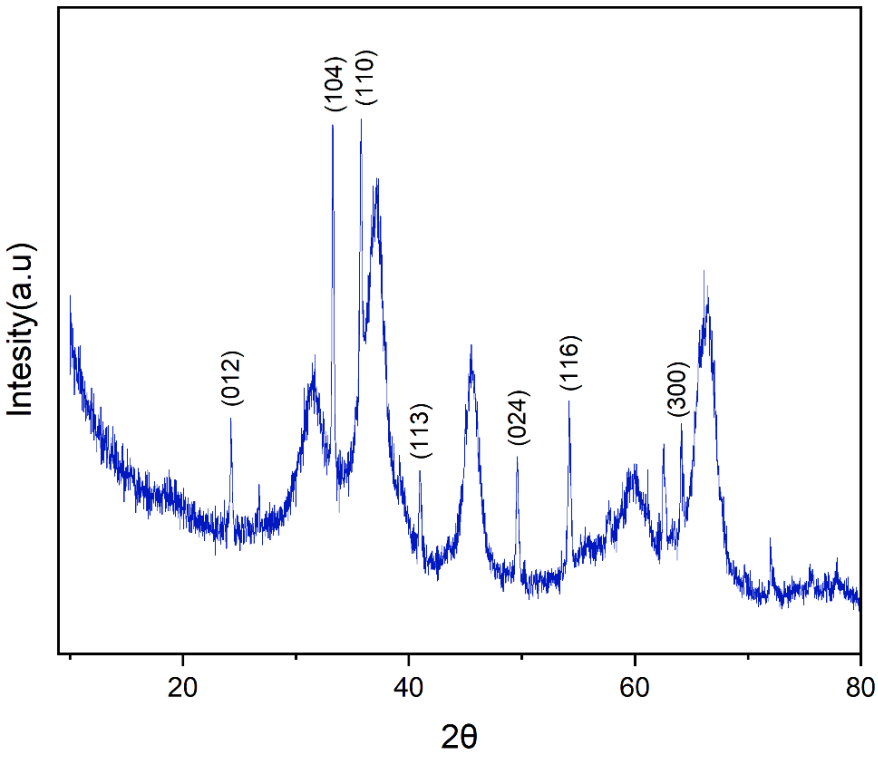

Figure 17. XRD pattern of the CVD-catalyst synthesized under inert atmosphere upon calcination at 300 °C for 12 h and at 600 °C for 24 h.

In addition, the XRD pattern for the nanocomposite catalyst with Fe_3O_4 revealed that the main phase was composed of Fe_2O_3. Other peaks can be attributed to impurities or to carbon bonds on the surface of the catalyst during preparation.

5.4.3 Ash content

The inorganic residue remaining after complete oxidation of organic material was evaluated and in Table 10 are presented the values obtained for the CNT samples and for the catalyst before heat treatment. Also, the values for the purified CNT and for the catalyst after heat treatment. Table 11 presents the difference between these two kinds of samples.

Table 10. Composition of ash content of the synthesized CNT materials and of the CVD-catalyst before heat treatment

Samples	Organic content (%)	Ash content (%)	Standard deviation
Catalyst_before	36.5	63.5	0.9
LDPE_600-40	41.6	58.4	0.1
LDPE_700-40	35.9	64.1	0.3
LDPE_800-40	36.8	63.2	0.4
HDPE_800-40	39.1	60.9	0.1
PP_800-40	36.6	63.4	0.2
MIX_800-40	37.9	62.1	0.4
Catalyst_after	7.1	92.9	0.6
P-LDPE_600-40	42.8	57.2	0.6
P-LDPE_700-40	86.0	14.0	0.4
P-LDPE_800-40	74.4	25.6	0.1
P-HDPE_800-40	81.7	18.3	0.5
P-PP_800-40	80.8	19.2	0.5
P-MIX_800-40	74.4	25.6	0.3

The catalyst before heat treatment presents similar results to those observed for CNTs. Subsequently, after heat treatment, the organic part is almost 7 % and the final product has the red color as Fe_2O_3. There are two suppositions about this lower percentage: it is only humidity, that can be verified by thermogravimetric analysis, or, during heat treatment, coke was formed and most of the carbon attaches on the surface.

For CNTs, LDPE_600-40 and LDPE_700-40 have extreme values, this can be visible on Table 11.

Table 11. Difference between before and after samples

Samples	Ash difference (%)
Catalyst	29.4
LDPE_600-40	1.2
LDPE_700-40	50.1
LDPE_800-40	37.6
HDPE_800-40	42.6
PP_800-40	44.2
MIX_800-40	36.5

The purification with sulfuric acid of LDPE_800-40 to MIX_800-40 resulted in significant reduction of ashes proving that the method could remove most of the inorganic compounds. 1.2% of difference on LDPE_600-40 can be an amorphous carbon formed in the heat treatment of the catalyst and, in CNT synthesis does not change.

In comparison with other studies of the same research group, the inert atmosphere influences largely the ash contents. Analyzing the "before" values obtained in Table 10 for the same temperature, the ashes percentage decrease according to following order: PP>LDPE>HDPE. Relating to the study previously performed in oxidative atmosphere[76], the reverse order was observed: HDPE>LDPE>PP. For the purified materials, the following order of ash content: LDPE>PP>HDPE while for the same previously reported study the order HDPE>PP>LDPE was found. Probably, the oxidative atmosphere made HDPE the highest ash contents, in contrast with inert atmosphere where HDPE has the lowest ash contents (before and after).

Considering the same CNT at Table 8. Yields obtained in the purification of the synthesized CNTs. And Table 10 for purified, the ash content follows the same order, P-LDPE_600-40 always have the biggest percentage due the possibility to have more iron catalyst than others.

5.4.4 FT-IR analysis

The FT-IR spectra of the purified (blue curve) and non-purified CNTs (black curve) are depicted in Figure 18 and Figure 19. The FT-IR spectra of the CVD-catalyst before heat treatment (black curve) and after heat treatment (blue curve) is shown in Figure 20.

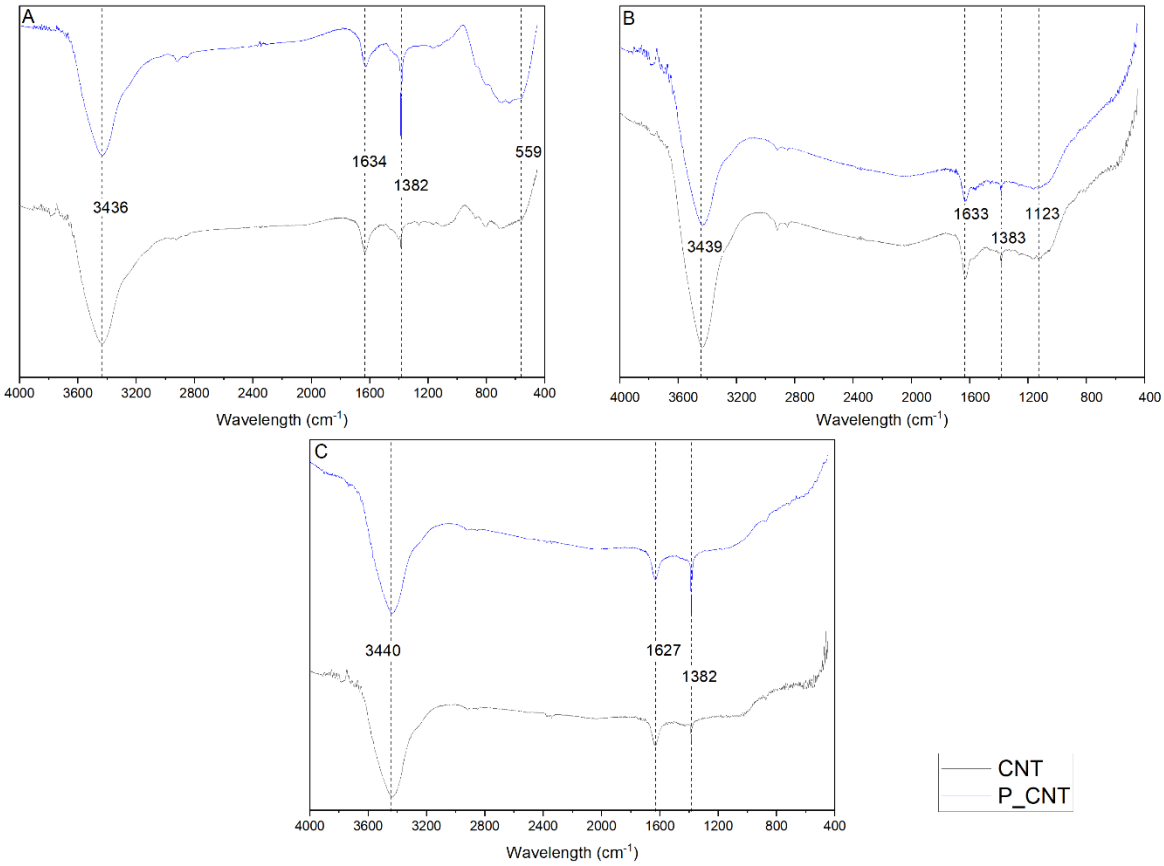

Figure 18. FT-IR spectra of a) LDPE_600-40, b) LDPE_700-40 and c) LDPE_800-40

In general, the strong peak between 3423 to 3440 cm^{-1} is attributed to the H–O stretching vibration of absorbed water on KBr and CNTs[64,77]. The obtained spectra are very similar, except for a more pronounced peak between 559 to 581 cm^{-1} corresponding to the Fe-O stretching vibration due to the presence of iron oxides[64,78]. Around 800 cm^{-1}, the vibration of Al–O bonds, especially AlO_4, are visible in black curves[79]. Vibrations of methylene (CH_2) and methyl (CH_3) are observed at 2926 cm^{-1} [80,81]. The bands between 1627 and 1639 cm^{-1} can be attributed to the stretching vibrations in carboxyls or carbonyls[80,82,83]. Sulfate groups appear between 1382 to 1385 cm^{-1} due to the treatment of the CNTs with sulfuric acid (blue curve)[84].

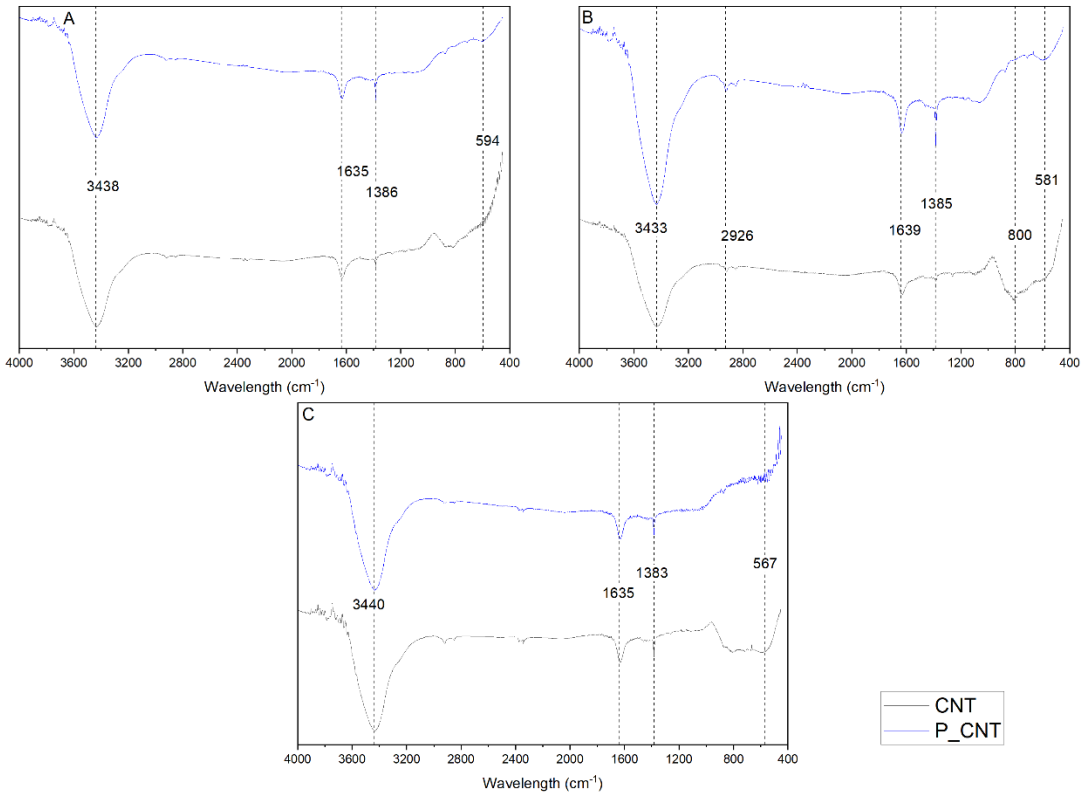

Figure 19. FT-IR spectra of a) HDPE_800-40, b) PP_800-40 and c) MIX_800-40

Seo et al, 2006[85] and Jiang et al, 2003[84], have also shown the two spectra of the CNTs that they produced, raw and purified. In both articles, are typically found the peaks defined in the CNT purification curves. In our research group, the CNTs peaks are similar, except for the small range corresponding to 2926 cm^{-1}.

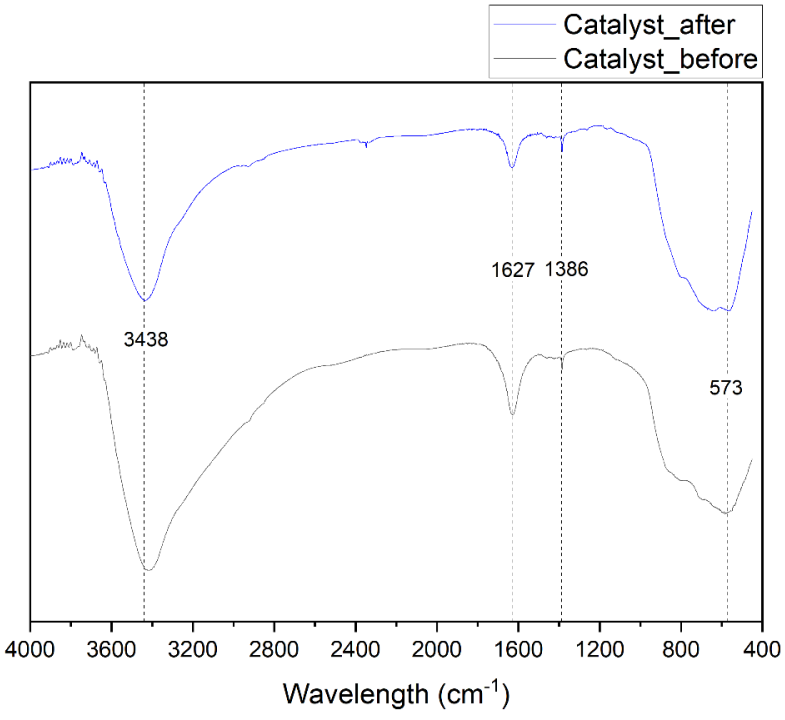

Figure 20. FT-IR spectra of the CVD-Catalyst

Moreover, it is observed that the peaks in the purified material were increased, especially the sulfate groups. Although the peaks that correspond to Fe-O and Al-O bonds have the amplitude minimized after the purification, except for the catalyst, since the heat treatment increases these bonds. The CVD-catalyst interacts with carbon, but there is no modification in magnetite, which can explain the rise of these groups.

Therefore, the FT-IR outcomes confirmed the iron oxide in the catalyst and in the nanotubes. These results indicate that the hydrogen bonding among the carboxylic and hydroxyl functional groups in CNTs may be the responsible for the assembly between the Fe_3O_4 nanoparticles. Also, some sulfate groups are attached to the molecule after purification.

5.4.5 Acidity and basicity

The surface acid-base chemical properties of the carbon materials were also determined, the corresponding values being gathered in Table 12.

Acid-base titration is a powerful tool for elucidating populations of functional groups with acid or basic characteristics at the surfaces of the CNTs[86].

Table 12. Results of the acidity and basicity characterization.

Samples	Acidity (µmol/g)	Basicity (µmol/g)
P-LDPE_600-40/1	855	0
P-LDPE_600-40/2	638	-
P-LDPE_800-40	199	0
P-HDPE_800-40	119	0
P-PP_800-40	0	0
P- MIX_800-40	179	0

P-LDPE_600-40, P-LDPE_800-40, P-HDPE_800-40 and P-MIX_800-40 possess an evident acid character, with a concentration of acidic functionalities higher than the concentration of basic functionalities. As expected, the materials resulting from the purification with sulfuric acid exhibit a pronounced acidic character[87]. Even though P-PP_800-40 does not present acidity, Figure 19-b), showed a peak in 1385 cm^{-1} for sulfonate groups.

Even with a duplicate, P-LDPE_600-40 showed a higher acidity, almost the same value as found by Delidovich et al, 2016[88], after the purification of the material in a stronger acid at 130 °C. A preferential location of the acidic sites of CNTs is related to the external surface facilitating accessibility. Ribeiro et al, 2013[87], reported graphite to

have a value of 190 µmol/g for acidity, almost the same values as found for P-LDPE_800-40, P-HDPE_800-40 and P-MIX_800-40. However, the values of basicity reported in the literature are different from zero.

As a result of the sulfuric acid, the oxidation can increase the acidity of CNTs, enabling them to be transformed morphologically[89,71]. The higher acidity of CNTs will lead to a lower number of available electrons at the carbon surface, since most of the oxygen-containing functionalities at the surface have an electron withdrawing capacity[90].

6 Conclusions and Future Research

6.1 Conclusions

The treatment of plastics to convert them into CNTs by sequential pyrolysis and CVD is viable at certain temperatures and flows. This study enabled to know the optimized parameters that better suits the process, specifically 40 mL/min of N_2 flow and 800 °C for LDPE. In addition, the purification of the materials prooved to be good to remove organic compounds at the CNTs surface. However, some sulfate groups attached to the surface are responsible by the acidity of the materials. These acid values must be considered for the final destination of CNTs and, the textural properties, such as S_{BET}, might have significant impact, since the access to the interior of some nanotubes would be possible through purification.

The synthesis of CVD-catalyst was done by the sol-gel method, obtaining a red dark catalyst. The use of this CVD-catalyst led to the production of magnetic CNTs. The washing process could remove the larger part of the organic content remaining from the structure of the CNT materials, proved by comparison of the Ash content before and after purification of the CNTs. However, the main phase is Fe_2O_3, as observed in XRD. That can be explained by coke formation, with the carbon attaching to the iron surface at the moment of heat treatment, also explaining the red dark color and, after the ash content, the red color. As only one catalyst was analyzed to produce CNTs, it was not possible to compare its efficiency with other catalysts, but the result was satisfactory due to the successful production of CNTs.

6.2 Future Research

Fifteen types of CNTs were synthesized using three different polymers and a mix of them. It would be interesting to do tests with a mix in different percentages of polymers and to increase the time in the setpoint temperature, to see if the CNT yield can be increased. Also, using real plastic material can give the idea of the plastic waste from MSW.

Certain functional groups can be removed following thermal treatment, to control the CNT surface chemistry, more than purification. Working at specific temperatures under an inert atmosphere, it is possible to remove selectively different types of surface groups[71].

When it comes to characterization, some analyses are required for better discussion about the nanotubes produced:

- Thermogravimetric analysis (TGA): can be used to assess the thermal stability of a material and to characterize its purity.
- Scanning electron microscopy (SEM): to obtain surface data and to see the type of CNTs grown.
- Transmission electron microscopy (TEM): to have a better knowledge of the carbon structures produced and of the CVD-catalyst.
- Raman Spectroscopy: analysis of thin structure electronic levels.

In addition, a study to identify and quantify the gases that left the furnace to the CVD section can also be done, using a gas chromatograph, allowing to study if the generated gases are harmful to the environment.

Bibliography

1. European Association Of Plastics Recycling. *Plastics-the Facts 2019 An Analysis of European Plastics Production, Demand and Waste Data*.; 2019.

2. Al-Salem SM, Antelava A, Constantinou A, Manos G, Dutta A. A review on thermal and catalytic pyrolysis of plastic solid waste (PSW). *J Environ Manage*. 2017;197:177-198. doi:10.1016/j.jenvman.2017.03.084

3. Jia J, Veksha A, Lim TT, Lisak G. In situ grown metallic nickel from X–Ni (X=La, Mg, Sr) oxides for converting plastics into carbon nanotubes: Influence of metal–support interaction. *J Clean Prod*. 2020;258. doi:10.1016/j.jclepro.2020.120633

4. Pedersen H, Elliott SD. Studying chemical vapor deposition processes with theoretical chemistry. *Theor Chem Acc*. 2014;133(5):1-10. doi:10.1007/s00214-014-1476-7

5. Wang J, Shen B, Lan M, Kang D, Wu C. Carbon nanotubes (CNTs) production from catalytic pyrolysis of waste plastics: The influence of catalyst and reaction pressure. *Catal Today*. 2020;351:50-57. doi:10.1016/j.cattod.2019.01.058

6. Miandad R, Barakat MA, Aburiazaiza AS, Rehan M, Nizami AS. Catalytic pyrolysis of plastic waste: A review. *Process Saf Environ Prot*. 2016;102:822-838. doi:10.1016/j.psep.2016.06.022

7. European Association Of Plastics Recycling. *Plastics-the Facts 2020 An Analysis of European Plastics Production, Demand and Waste Data*.; 2020.

8. Mano EB, Mendes LC. *Introdução a Polímeros*. Vol 1. EDITORA EDGARD BLÜCHER; 2004.

9. PlasticsEurope. *Annual Review 2017-2018*. Vol 15.; 2018. https://www.plasticseurope.org/download_file/force/1830/181

10. Council of the European Union. Joint Declaration of the Prague Eastern Partnership Summit. Published 2013. http://www.consilium.europa.eu/uedocs/cms_data/docs/pressdata/en/er/107589.pdf

11. *Directive 2008/122/EC of the European Parliament and of the Council of 19 November 2008 on Waste and Repealing Certain Directives*.; 2008:3-30. doi:10.5040/9781782258674.0028

12. Singh N, Hui D, Singh R, Ahuja IPS, Feo L, Fraternali F. Recycling of plastic solid waste: A state of art review and future applications. *Compos Part B Eng*. 2017;115:409-422. doi:10.1016/j.compositesb.2016.09.013

13. Al-Salem SM, Lettieri P, Baeyens J. Recycling and recovery routes of plastic solid waste (PSW): A review. *Waste Manag*. 2009;29(10):2625-2643. doi:10.1016/j.wasman.2009.06.004

14. Zhuo C, Levendis YA. Upcycling waste plastics into carbon nanomaterials: A review. *J Appl Polym Sci*. 2014;131(4). doi:10.1002/app.39931

15. Sharma SS, Batra VS. Production of hydrogen and carbon nanotubes via catalytic thermo-chemical conversion of plastic waste: review. *J Chem Technol Biotechnol*. 2020;95(1):11-19. doi:10.1002/jctb.6193

16. Yang RX, Wu SL, Chuang KH, Wey MY. Co-production of carbon nanotubes and hydrogen from waste plastic gasification in a two-stage fluidized catalytic bed. *Renew Energy*. 2020;159:10-22. doi:10.1016/j.renene.2020.05.141

17. Zhang Y, Ji G, Ma D et al, Exergy and energy analysis of pyrolysis of plastic wastes in rotary kiln with heat carrier. *Process Saf Environ Prot*. 2020;142:203-211. doi:10.1016/j.psep.2020.06.021

18. Singh RK, Ruj B, Sadhukhan AK, Gupta P. Conventional pyrolysis of Plastic waste for Product recovery and utilization of pyrolytic gases for carbon nanotubes production. *Environ Sci Pollut Res*. Published online 2020. doi:10.1007/s11356-020-11204-1

19. Almeida D, De Fátima Marques M. Thermal and catalytic pyrolysis of plastic waste. *Polimeros*. 2016;26(1):44-51. doi:10.1590/0104-1428.2100

20. López A, de Marco I, Caballero BM, Laresgoiti MF, Adrados A. Influence of time and temperature on pyrolysis of plastic wastes in a semi-batch reactor. *Chem Eng J*. 2011;173(1):62-71. doi:10.1016/j.cej.2011.07.037

21. Miandad R, Barakat MA, Aburiazaiza AS, Rehan M, Ismail IMI, Nizami AS. Effect of plastic waste types on pyrolysis liquid oil. *Int Biodeterior Biodegrad*. 2017;119:239-252. doi:10.1016/j.ibiod.2016.09.017

22. Kumagai S, Yoshioka T. Feedstock recycling via waste plastic pyrolysis. *J Japan Pet Inst*. 2016;59(6):243-253. doi:10.1627/jpi.59.243

23. Abebe Abide T. Recovery of Liquid Hydrocarbon Fuels from Polypropylene Waste Plastics via Catalytic Pyrolysis. *J Catal Catal*. 2020;7(1):33-48.

24. Parku GK, Collard FX, Görgens JF. Pyrolysis of waste polypropylene plastics for energy recovery: Influence of heating rate and vacuum conditions on composition of fuel product. *Fuel Process Technol*. 2020;209(March):36-38. doi:10.1016/j.fuproc.2020.106522

25. Luo S, Xiao B, Hu Z, Liu S. Effect of particle size on pyrolysis of single-component municipal solid waste in fixed bed reactor. *Int J Hydrogen Energy*. 2010;35(1):93-97. doi:10.1016/j.ijhydene.2009.10.048

26. Anzar N, Hasan R, Tyagi M, Yadav N, Narang J. Carbon nanotube - A review on Synthesis, Properties and plethora of applications in the field of biomedical science. *Sensors Int*. 2020;1:100003. doi:10.1016/j.sintl.2020.100003

27. Shah KA, Tali BA. Synthesis of carbon nanotubes by catalytic chemical vapour deposition: A review on carbon sources, catalysts and substrates. *Mater Sci Semicond Process*. 2016;41:67-82. doi:10.1016/j.mssp.2015.08.013

28. Panchakarla LS, Rao CNR. Nanotubes. In: *Advances in the Chemistry and Physics of Materials*. ; 2019:1-26. doi:10.1142/9789811211331_0001

29. Purohit R, Purohit K, Rana S, Rana RS, Patel V. Carbon Nanotubes and Their Growth Methods. *Procedia Mater Sci*. 2014;6(Icmpc):716-728. doi:10.1016/j.mspro.2014.07.088

30. Yang P, ZHENG B, LIU J. Cvd Synthesis of Single-Walled Carbon Nanotubes. *Chem Nanostructured Mater*. 2003;2(1):101-125. doi:10.1142/9789812560049_0004

31. Ghaemi F, Ali M, Yunus R, Othman RN. *Synthesis of Carbon Nanomaterials Using Catalytic Chemical Vapor Deposition Technique*. Elsevier Inc.; 2018. doi:10.1016/B978-0-12-815757-2.00001-2

32. Kirihara S, Kazuhiro N. *Multi-Dimensional Additive Manufacturing*. (Kirihara S, Kazuhiro N, eds.). Springer Singapore; 2021. doi:10.1007/978-981-15-7910-3

33. Wang X-D, Vinodgopal K, Dai G-P. Synthesis of Carbon Nanotubes by Catalytic Chemical Vapor Deposition. *Intechopen*. 2020;(Cell Interaction-Regulation of Immune Responses, Disease Development and Management Strategies):1-15. https://www.intechopen.com/books/advanced-biometric-technologies/liveness-detection-in-biometrics

34. Bajad G, Vijayakumar RP, Rakhunde P, Hete A, Bhade M. Processing of mixed-plastic waste to fuel oil, carbon nanotubes and hydrogen using multi–core reactor. *Chem Eng Process Process*

Intensif. 2017;121:205-214. doi:10.1016/j.cep.2017.09.011

35. Zhuo C, Hall B, Richter H, Levendis Y. Synthesis of carbon nanotubes by sequential pyrolysis and combustion of polyethylene. *Carbon N Y*. 2010;48(14):4024-4034. doi:10.1016/j.carbon.2010.07.007

36. Tripathi PK, Durbach S, Coville NJ. Synthesis of Multi-Walled carbon nanotubes from plastic waste using a Stainless-Steel CVD reactor as catalyst. *Nanomaterials*. 2017;7(10). doi:10.3390/nano7100284

37. Yao D, Wu C, Yang H et al, Co-production of hydrogen and carbon nanotubes from catalytic pyrolysis of waste plastics on Ni-Fe bimetallic catalyst. *Energy Convers Manag*. 2017;148:692-700. doi:10.1016/j.enconman.2017.06.012

38. Kong Q, Zhang J. Synthesis of straight and helical carbon nanotubes from catalytic pyrolysis of polyethylene. *Polym Degrad Stab*. 2007;92(11):2005-2010. doi:10.1016/j.polymdegradstab.2007.08.002

39. Barbarias I, Artetxe M, Lopez G, Arregi A, Bilbao J, Olazar M. Influence of the conditions for reforming HDPE pyrolysis volatiles on the catalyst deactivation by coke. *Fuel Process Technol*. 2018;171:100-109. doi:10.1016/j.fuproc.2017.11.003

40. Jiang Z, Song R, Bi W, Lu J, Tang T. Polypropylene as a carbon source for the synthesis of multi-walled carbon nanotubes via catalytic combustion. *Carbon N Y*. 2007;45(2):449-458. doi:10.1016/j.carbon.2006.08.012

41. Yang RX, Chuang KH, Wey MY. Effects of Nickel Species on Ni/Al_2O_3 Catalysts in Carbon Nanotube and Hydrogen Production by Waste Plastic Gasification: Bench- and Pilot-Scale Tests. *Energy and Fuels*. 2015;29(12):8178-8187. doi:10.1021/acs.energyfuels.5b01866

42. Yao D, Yang H, Hu Q, Chen Y, Chen H, Williams PT. Carbon nanotubes from post-consumer waste plastics: Investigations into catalyst metal and support material characteristics. *Appl Catal B Environ*. 2021;280. doi:10.1016/j.apcatb.2020.119413

43. Yao D, Zhang Y, Williams PT, Yang H, Chen H. Co-production of hydrogen and carbon nanotubes from real-world waste plastics: Influence of catalyst composition and operational parameters. *Appl Catal B Environ*. 2018;221:584-597. doi:10.1016/j.apcatb.2017.09.035

44. Liu X, Zhang Y, Nahil MA, Williams PT, Wu C. Development of Ni- and Fe- based catalysts with different metal particle sizes for the production of carbon nanotubes and hydrogen from thermo-chemical conversion of waste plastics. *J Anal Appl Pyrolysis*. 2017;125:32-39. doi:10.1016/j.jaap.2017.05.001

45. Yang Z, Zhang Q, Luo G, Huang JQ, Zhao MQ, Wei F. Coupled process of plastics pyrolysis and chemical vapor deposition for controllable synthesis of vertically aligned carbon nanotube arrays. *Appl Phys A Mater Sci Process*. 2010;100(2):533-540. doi:10.1007/s00339-010-5868-9

46. Yao D, Yang H, Chen H, Williams PT. Investigation of nickel-impregnated zeolite catalysts for hydrogen/syngas production from the catalytic reforming of waste polyethylene. *Appl Catal B Environ*. 2018;227:477-487. doi:10.1016/j.apcatb.2018.01.050

47. Gohier A, Ewels CP, Minea TM, Djouadi MA. Carbon nanotube growth mechanism switches from tip- to base-growth with decreasing catalyst particle size. *Carbon N Y*. 2008;46(10):1331-1338. doi:10.1016/j.carbon.2008.05.016

48. Prasek J, Drbohlavova J, Chomoucka J et al, Methods for carbon nanotubes synthesis - Review. *J Mater Chem*. 2011;21(40):15872-15884. doi:10.1039/c1jm12254a

49. Suan MSM, Chin CK, Raza JA, Hasib H, Abid MA 'Azam M, Nurdin I. Synthesis and Characterizations of Fe_3O_4 Added with Al2O3 Nanoparticles via Sol-Gel Technique. 2020;2.

doi:10.1088/1757-899X/957/1/012040

50. Xi Liua, Xuea L, Chena X et al, IRON OXIDE AND Fe_2O_3/Al_2O_3 USED TO CATALYZE REMOVING HYDROGEN FROM TAIL CHLORINE AT LOW TEMPERATURE. *Quim Nova, Vol 42, No 3, 319-328*. 2019;42(3):319-328.

51. Shi D, Cheng JP, Liu F, Zhang XB. Controlling the size and size distribution of magnetite nanoparticles on carbon nanotubes. *J Alloys Compd*. 2010;502(2):365-370. doi:10.1016/j.jallcom.2010.04.169

52. Ward DA, Ko EI. Preparing Catalytic Materials by the Sol-Gel Method. *Ind Eng Chem Res*. 1995;34(2):421-433. doi:10.1021/ie00041a001

53. Porro S, Musso S, Giorcelli M, Chiodoni A, Tagliaferro A. Optimization of a thermal-CVD system for carbon nanotube growth. *Phys E Low-Dimensional Syst Nanostructures*. 2007;37(1-2):16-20. doi:10.1016/j.physe.2006.07.010

54. Malgas GF, Arendse CJ, Cele NP, Cummings FR. Effect of mixture ratios and nitrogen carrier gas flow rates on the morphology of carbon nanotube structures grown by CVD. *J Mater Sci*. 2008;43(3):1020-1025. doi:10.1007/s10853-007-2230-5

55. Panahi A, Sun X, Song G, Levendis YA. On the Influences of Carrier Gas Type and Flow Rate on CVD Synthesis of CNTs from Postconsumer Polyethylene. *Ind Eng Chem Res*. 2020;59(31):14004-14014. doi:10.1021/acs.iecr.0c02000

56. Aboul-Enein AA, Adel-Rahman H, Haggar AM, Awadallah AE. Simple method for synthesis of carbon nanotubes over Ni-Mo/Al_2O_3 catalyst via pyrolysis of polyethylene waste using a two-stage process. *Fullerenes Nanotub Carbon Nanostructures*. 2017;25(4):211-222. doi:10.1080/1536383X.2016.1277422

57. Kumar M, Ando Y. Chemical vapor deposition of carbon nanotubes: A review on growth mechanism and mass production. *J Nanosci Nanotechnol*. 2010;10(6):3739-3758. doi:10.1166/jnn.2010.2939

58. Diaz de Tuesta JL, F. Machado B, Serp P, Adrián AM, Faria JL, T. Gomes H. Janus amphiphilic carbon nanotubes as Pickering interfacial catalysts for the treatment of oily wastewater by selective oxidation with hydrogen peroxide. *Catal Today*. 2020;356:205-215. doi:10.1016/J.CATTOD.2019.07.012

59. Sharma SK, Verma DS, Khan LU, Kumar S, Khan SB. Fourier Transform Infrared Spectroscopy: Fundamentals and Application in Functional Groups and Nanomaterials Characterization. In: *Handbook of Materials Characterization*. ; 2018:1-613. doi:10.1007/978-3-319-92955-2

60. Cardoso J, Gomes HT, Brito P. Viability of the use of leachates from a mechanical biological municipal solid waste treatment plant as fertilizers. *Recycling*. 2019;4(1). doi:10.3390/recycling4010008

61. Silva AS, Kalmakhanova MS, Massalimova BK, de Tuesta JLD, Gomes HT. Wet peroxide oxidation of paracetamol using acid activated and Fe/Co-pillared clay catalysts prepared from natural clays. *Catalysts*. 2019;9(9). doi:10.3390/catal9090705

62. Kohli R, Mittal KL. Methods for Assessing Surface Cleanliness. In: *Developments in Surface Contamination and Cleaning*. Vol 12. ; 2019:23-105. doi:10.1016/b978-0-12-816081-7.00003-6

63. Thommes M, Kaneko K, Neimark A V. et al, Physisorption of gases, with special reference to the evaluation of surface area and pore size distribution (IUPAC Technical Report). *Pure Appl Chem*. 2015;87(9-10):1051-1069. doi:10.1515/pac-2014-1117

64. Tavousi A, Ahmadi E, Mohammadi-Behzad L, Riahifar V, Maghemi F. Sensitive electrochemical sensor using polypyrrole-coated Fe_3O_4 core-shell nanoparticles/multiwall carbon nanotubes

modified graphite electrode for atorvastatin analysis. *Microchem J*. 2020;158(June):105159. doi:10.1016/j.microc.2020.105159

65. Liu P, He S, Wei H, Wang J, Sun C. Characterization of α-Fe_2O_3/γ-Al_2O_3 catalysts for catalytic wet peroxide oxidation of m-Cresol. *Ind Eng Chem Res*. 2015;54(1):130-136. doi:10.1021/ie5037897

66. Li Y-H, Wang S, Zhang X et al, Adsorption of ¯uoride from water by aligned carbon nanotubes. doi:10.1016/S0025-5408(02)01063-2

67. Dasgupta K, Kar S, Venugopalan R et al, Self-standing geometry of aligned carbon nanotubes with high surface area. Published online 2007. doi:10.1016/j.matlet.2007.10.057

68. Basheer AO, Alsaadi MA, Zuhairi W, Yaacob W. Carbon Nanotubes by Chemical Vapor Deposition : Application for Aluminum Removal. *Polymers (Basel)*. 2020;12(6):18. doi:10.3390/polym12061305

69. Niu JJ, Wang JN, Jiang Y, Su LF, Ma J. An approach to carbon nanotubes with high surface area and large pore volume. *Microporous Mesoporous Mater*. 2007;100(1-3):1-5. doi:10.1016/j.micromeso.2006.10.009

70. Peigney A, Laurent C, Flahaut E, Bacsa RR, Rousset A. Specific surface area of carbon nanotubes and bundles of carbon nanotubes. *Carbon N Y*. 2001;39:507. doi:10.1016/S0008-6223(00)00155-X

71. Martin-Martinez M, Machado BF, Serp P et al, Carbon nanotubes as catalysts for wet peroxide oxidation: The effect of surface chemistry. *Catal Today*. 2020;357(March):332-340. doi:10.1016/j.cattod.2019.03.014

72. Zhang D, Shi L, Fang J, Li X, Dai K. Preparation and modification of carbon nanotubes. *Mater Lett*. 2005;59(29-30):4044-4047. doi:10.1016/j.matlet.2005.07.081

73. Li Q, Deng L, Kim J-K et al, Growth of Carbon Nanotubes on Electrospun Cellulose Fibers for High Performance Supercapacitors. *J Electrochem Soc*. 2017;164(13):A3220-A3228. doi:10.1149/2.1181713jes

74. Wu SL, Chen CM, Kuo JH, Wey MY. Synthesis of carbon nanotubes with controllable diameter by chemical vapor deposition of methane using Fe@Al_2O_3 core–shell nanocomposites. *Chem Eng Sci*. 2020;217:115541. doi:10.1016/j.ces.2020.115541

75. Khodadadi A, Farahmandjou M, Yaghoubi M. Investigation on synthesis and characterization of Fe-doped Al2O3 nanocrystals by new sol–gel precursors. *Chem Eng J*. 2019;5:0-35.

76. Sanches LF. Valorisation of carbon-rich solid wastes into nanostructured catalysts for wet peroxide oxidation of contaminants of emerging concern. Published online 2021.

77. Fan XJ, Li X. Preparation and magnetic properties of multiwalled carbon nanotubes decorated by Fe_3O_4 nanoparticles. *Xinxing Tan Cailiao/New Carbon Mater*. 2012;27(2):111-116. doi:10.1016/S1872-5805(12)60007-9

78. Raghu MS, Yogesh Kumar K, Prashanth MK, Prasanna BP, Vinuth R, Pradeep Kumar CB. Adsorption and antimicrobial studies of chemically bonded magnetic graphene oxide-Fe3O4 nanocomposite for water purification. *J Water Process Eng*. 2017;17:22-31. doi:10.1016/j.jwpe.2017.03.001

79. Kazemifard S, Nayebzadeh H, Saghatoleslami N, Safakish E. Assessment the activity of magnetic KOH/Fe_3O_4@Al_2O_3 core–shell nanocatalyst in transesterification reaction: effect of Fe/Al ratio on structural and performance. *Environ Sci Pollut Res*. 2018;25(32):32811-32821. doi:10.1007/s11356-018-3249-7

80. Wang L, Ge L, Rufford TE et al, A comparison study of catalytic oxidation and acid oxidation to

prepare carbon nanotubes for filling with Ru nanoparticles. *Carbon N Y*. 2011;49(6):2022-2032. doi:10.1016/j.carbon.2011.01.028

81. Chen J, Wang Y, Huang Y et al, Magnetic multiwall carbon nanotubes modified with dual hydroxy functional ionic liquid for the solid-phase extraction of protein. *Analyst*. 2015;140(10):3474-3483. doi:10.1039/c5an00201j

82. Naganathan D, Thangamani P, Selvam T, Narayanasamy T. Ce doped ZnO/f-MWCNT moss ball like nanocomposite: a strategy for high responsive current detection of L-tryptophan. *Microchim Acta*. 2018;185(2). doi:10.1007/s00604-017-2641-1

83. Ramezan zadeh MH, Seifi M, Hekmatara H, Askari MB. Preparation and study of the electrical, magnetic and thermal properties of Fe_3O_4 coated carbon nanotubes. *Chinese J Phys*. 2017;55(4):1319-1328. doi:10.1016/j.cjph.2017.06.011

84. Jiang K, Eitan A, Schadler LS et al, Selective attachment of gold nanoparticles to nitrogen-doped carbon nanotubes. *Nano Lett*. 2003;3(3):275-277. doi:10.1021/nl025914t

85. Seo DW, Yoon WJ, Park SJ, Jo MC, Kim JS. The Preparation of Multi-walled CNT–PMMA Nanocomposite. 2006;7(4):266-270.

86. Kim YS, Park CR. One-pot titration methodology for the characterization of surface acidic groups on functionalized carbon nanotubes. *Carbon N Y*. 2016;96:729-741. doi:10.1016/j.carbon.2015.08.078

87. Ribeiro RS, Silva AMT, Figueiredo JL, Faria JL, Gomes HT. The influence of structure and surface chemistry of carbon materials on the decomposition of hydrogen peroxide. *Carbon N Y*. 2013;62:97-108. doi:10.1016/j.carbon.2013.06.001

88. Delidovich I, Palkovits R. Impacts of acidity and textural properties of oxidized carbon materials on their catalytic activity for hydrolysis of cellobiose. *Microporous Mesoporous Mater*. 2016;219:317-321. doi:10.1016/j.micromeso.2015.07.011

89. Hanelt S, Orts-Gil G, Friedrich JF, Meyer-Plath A. Differentiation and quantification of surface acidities on MWCNTs by indirect potentiometric titration. *Carbon N Y*. 2011;49(9):2978-2988. doi:10.1016/j.carbon.2011.03.016

90. Karimi M, Silva JAC, Gonçalves CNDP, Diaz De Tuesta JL, Rodrigues AE, Gomes HT. CO2 Capture in Chemically and Thermally Modified Activated Carbons Using Breakthrough Measurements: Experimental and Modeling Study. *Ind Eng Chem Res*. 2018;57(32):11154-11166. doi:10.1021/acs.iecr.8b00953

7 ANNEXES

7.1 Effect of N_2 inlet flow in the heating rate of the tubular furnace

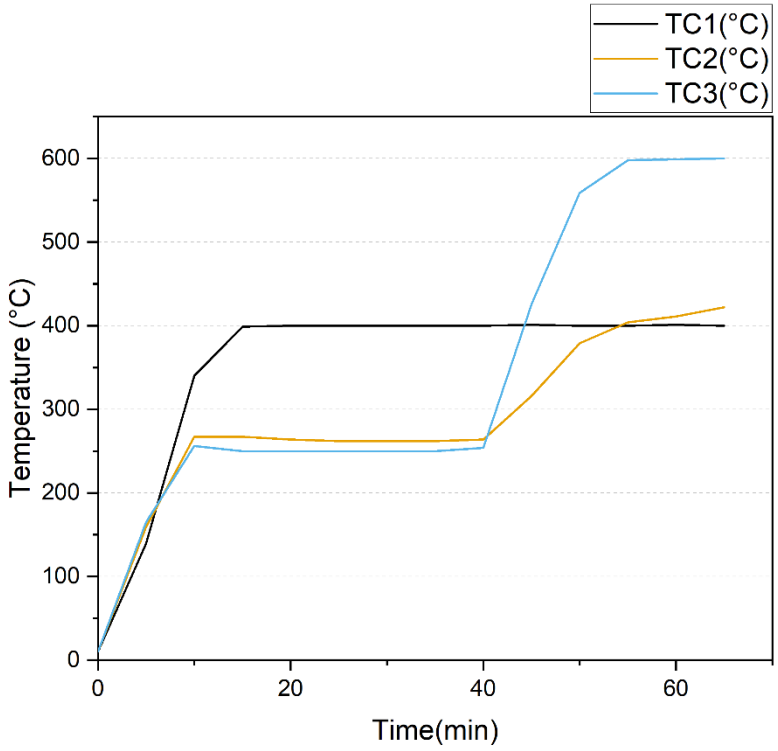

Figure 21. 25 mL/min with 400 °C in the superior zone and 600 °C in the inferior zone

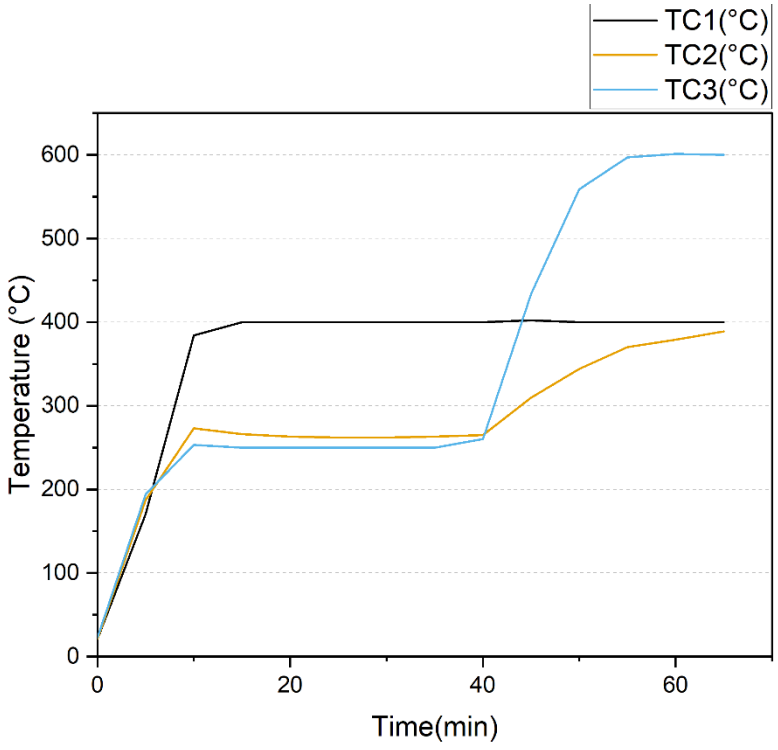

Figure 22. 40 mL/min with 400 °C in the superior zone and 600 °C in the inferior zone

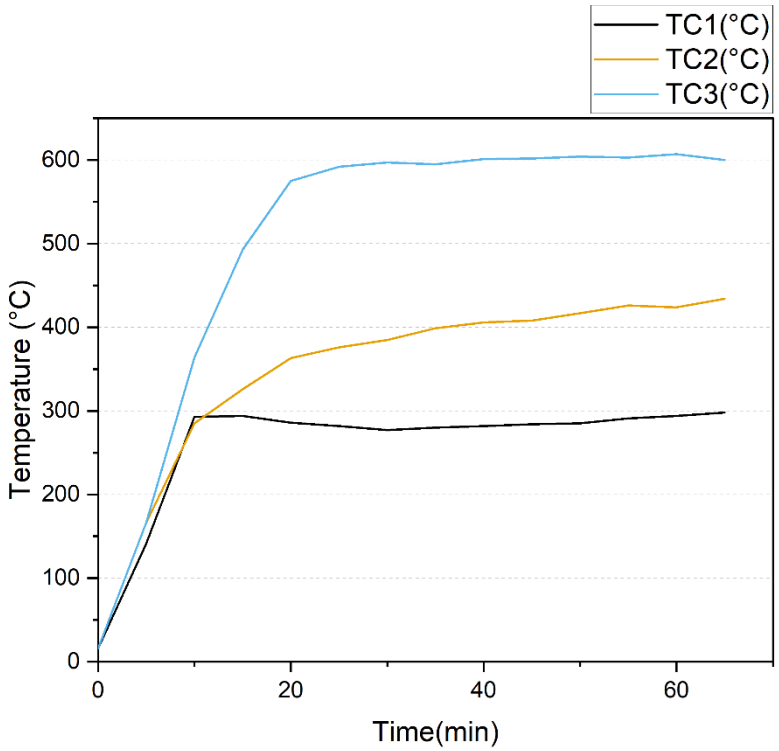

Figure 23. 25 mL/min with 600 °C in the inferior zone

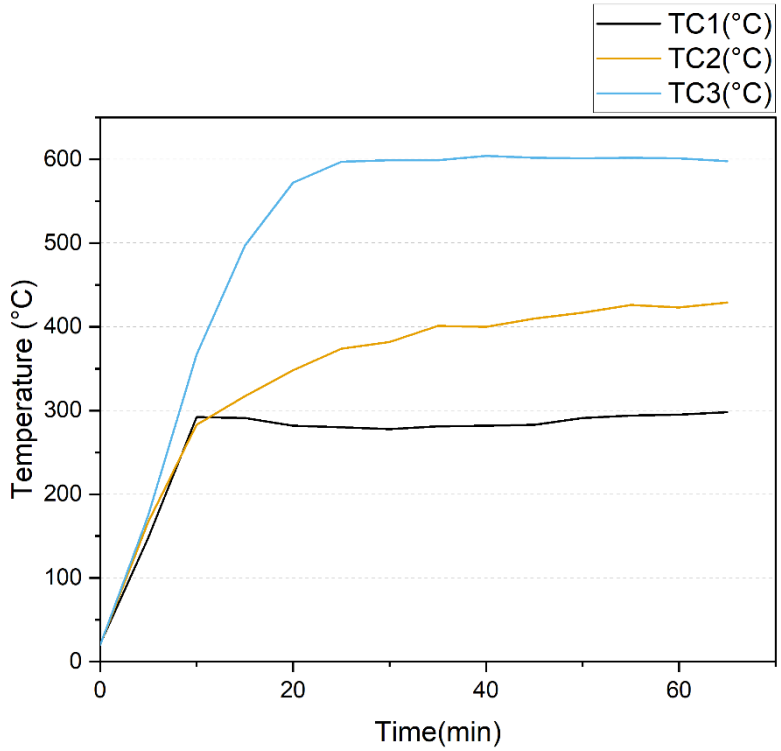

Figure 24. 40 mL/min with 600 °C in the inferior zone

7.2 Effect of retention time

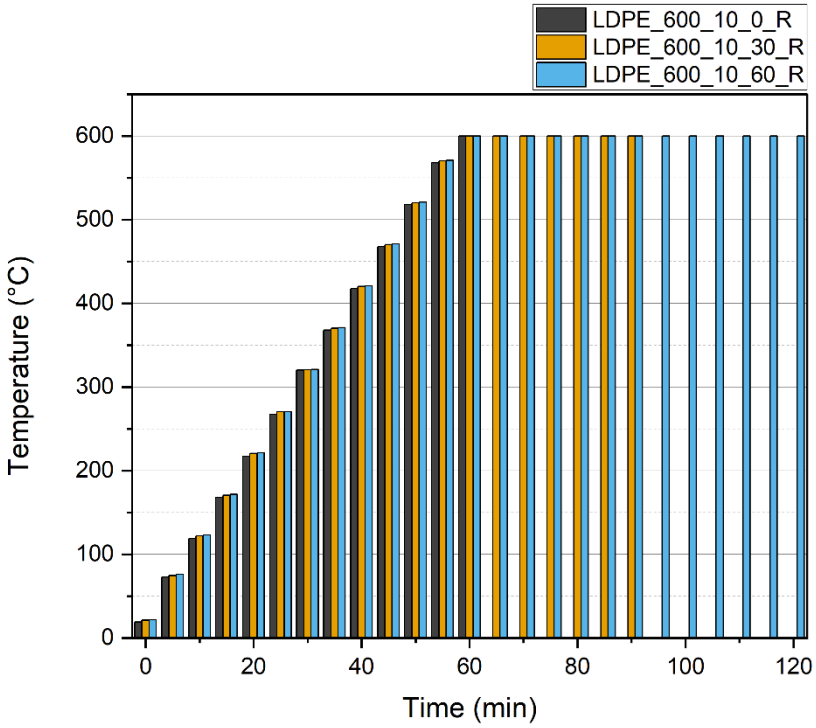

Figure 25. Effect of the retention time on the temperature response upon heating the oven until 600 ºC at 10 °C/min with LDPE.

7.3 Residues

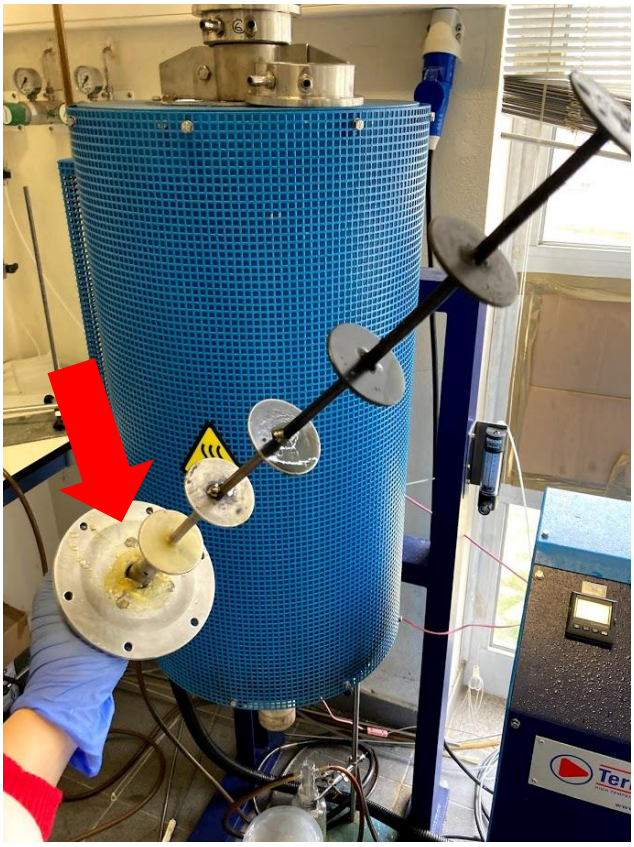

Figure 26. Wax as residue of CNTs production

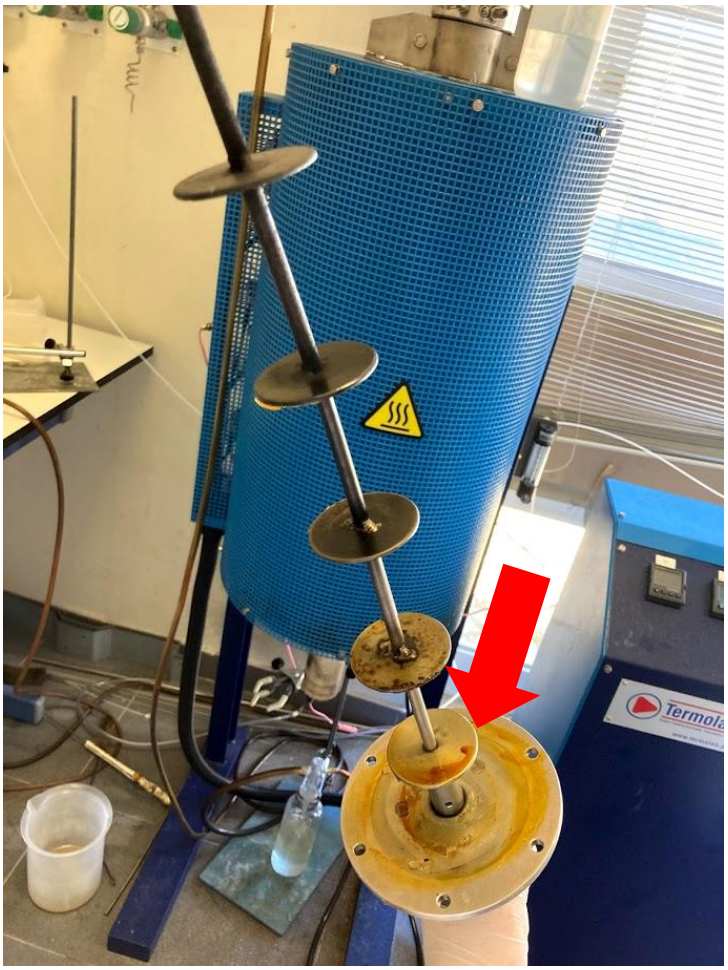

Figure 27.Oil as a residue in CNTs production

7.4 Fe_3O_4/Al_2O_3 yield

- Theoretical mass of iron:

For $FeCl_2$, the mass used was 1.98866 g. Molecular weight is 198.80 g/mol. So, the total number of mols is:

$$n = \frac{1.98866}{198.80} = 0.01\ mol$$

The molar mass of Fe is 55.845 g/mol. Dividing mols by molar mass, results in a mass of Fe inside this molecule.

$$m = \frac{0.010005533}{55.845} = \ 0.559\ g$$

For $FeCl_3$, the mass used was 5.4066 g. The molecular weight is 270.29 g/mol. So, the total number of mols is:

$$n = \frac{5.4066}{270.29} = 0.02\ mol$$

The molar mass of Fe is 55.845 g/mol. Dividing mols by molar mass, results in a mass of Fe inside this molecule.

$$m = \frac{0.02000296}{55.845} = 1.117\ g$$

Then, the theoretical Fe mass is $0.559\ g + 1.117\ g$, given by 1.676 g. And, to discover the percentage of Fe inside the initial mixture, sum the initial weight of $FeCl_2$ and $FeCl_3$: 7.3957 g.

7.3957 g – 100%

1.676 g - x

x= 22.66%

- Experimental mass of iron:

Taking the average mass of all catalysts synthetized, that was 6.688107 g, the experimental percentage of iron is found:

6.688107 g – 100%

1.676 g - x

x= 25.06%